Article

Molecular Cell

C1QBP Promotes Homologous Recombination by Stabilizing MRE11 and Controlling the Assembly and Activation of MRE11/RAD50/NBS1 Complex

Graphical Abstract

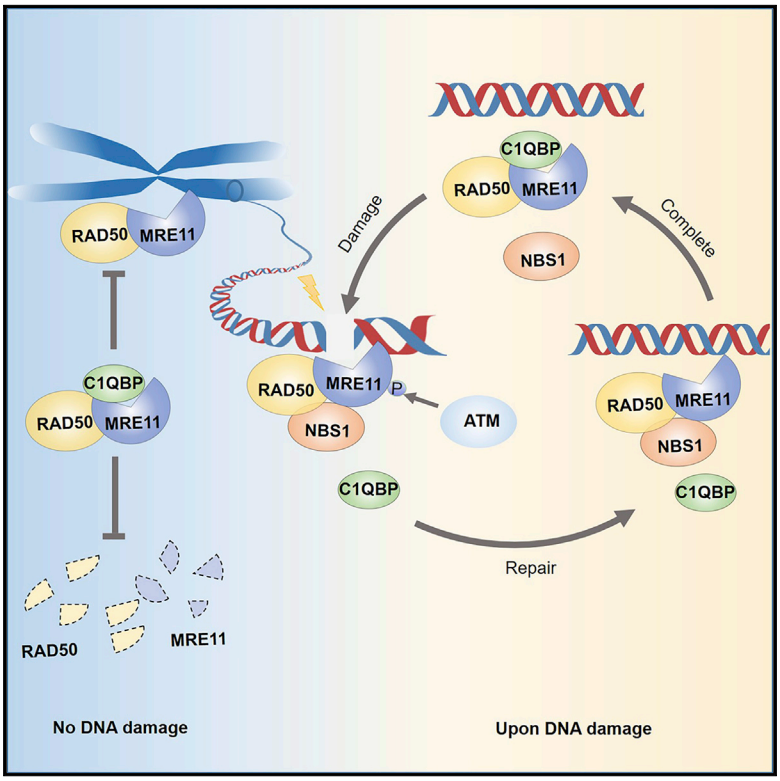

Authors

Yongtai Bai, Weibin Wang, Siyu Li, ..., Wei-Guo Zhu, Xingzhi Xu, Jiadong Wang

Correspondence

wangjd@bjmu.edu.cn

In Brief

The MRE11/RAD50/NBS1 (MRN) complex plays a critical role in the initial processing of DNA double-strand breaks. Bai et al. show that C1QBP functions as a molecular sponge, which maintains MRE11 protein stability, while controlling the assembly and activation of the MRN complex for efficient DNA damage repair.

Highlights

- C1QBP stabilizes the MRE11 protein by forming the MRC complex with MRE11/RAD50
- C1QBP inhibits MRE11 exonuclease activity by preventing its binding to DNA
- Appropriate C1QBP levels are essential for genomic stability and DNA repair

Bai et al., 2019, Molecular Cell *75*, 1–16
September 19, 2019
https://doi.org/10.1016/j.molcel.2019.06.023

CellPress

Please cite this article in press as: Bai et al., C1QBP Promotes Homologous Recombination by Stabilizing MRE11 and Controlling the Assembly and Activation of MRE11/RAD50/NBS1 Complex, Molecular Cell (2019), https://doi.org/10.1016/j.molcel.2019.06.023

Molecular Cell
Article

C1QBP Promotes Homologous Recombination by Stabilizing MRE11 and Controlling the Assembly and Activation of MRE11/RAD50/NBS1 Complex

Yongtai Bai,[1,7] Weibin Wang,[1,7] Siyu Li,[1,7] Jun Zhan,[2,7] Hanxiao Li,[1] Meimei Zhao,[1] Xiao Albert Zhou,[1] Shiwei Li,[1] Xiaoman Li,[1] Yanfei Huo,[1] Qinjian Shen,[1] Mei Zhou,[1] Hongquan Zhang,[2] Jianyuan Luo,[3] Patrick Sung,[4,5] Wei-Guo Zhu,[6] Xingzhi Xu,[6] and Jiadong Wang[1,8,*]

[1]Department of Radiation Medicine, Institute of Systems Biomedicine, School of Basic Medical Sciences, Peking University Health Science Center, Beijing 100191, China
[2]Department of Anatomy, Histology and Embryology, School of Basic Medical Sciences, Peking University Health Science Center, Beijing 100191, China
[3]Department of Biochemistry and Molecular Biology, School of Basic Medical Sciences, Peking University Health Science Center, Beijing 100191, China
[4]Department of Molecular Biophysics and Biochemistry, Yale University School of Medicine, New Haven, CT 06520, USA
[5]Department of Biochemistry and Structural Biology, University of Texas Health Science Center at San Antonio, San Antonio, TX 78229, USA
[6]Department of Biochemistry and Molecular Biology, Shenzhen University Health Science Center, Shenzhen, 518060, China
[7]These authors contributed equally
[8]Lead Contact
*Correspondence: wangjd@bjmu.edu.cn
https://doi.org/10.1016/j.molcel.2019.06.023

SUMMARY

MRE11 nuclease forms a trimeric complex (MRN) with RAD50 and NBS1 and plays a central role in preventing genomic instability. When DNA double-strand breaks (DSBs) occur, MRN is quickly recruited to the damage site and initiates DNA end resection; accordingly, MRE11 must be tightly regulated to avoid inefficient repair or nonspecific resection. Here, we show that MRE11 and RAD50 form a complex (MRC) with C1QBP, which stabilizes MRE11/RAD50, while inhibiting MRE11 nuclease activity by preventing its binding to DNA or chromatin. Upon DNA damage, ATM phosphorylates MRE11-S676/S678 to quickly dissociate the MRC complex. Either excess or insufficient C1QBP impedes the recruitment of MRE11 to DSBs and impairs the DNA damage response. C1QBP is highly expressed in breast cancer and positively correlates with MRE11 expression, and the inhibition of C1QBP enhances tumor regression with chemotherapy. By influencing MRE11 at multiple levels, C1QBP is, thus, an important player in the DNA damage response.

INTRODUCTION

Maintaining genomic stability is essential for cellular survival and accurate transmission of genetic materials to future generations. Endogenous and exogenous DNA damage and imprecise DNA replication are major sources of genomic instability in cells. By processing multiple aspects of the DNA damage response (DDR), such as initial DSB detection, DNA end resection, signal transduction, and promotion of DSB repair, the MRE11/RAD50/NBS1 (MRN) complex is the crucial factor maintaining genomic stability (Assenmacher and Hopfner, 2004; Cejka, 2015; Paull, 2018; Paull and Deshpande, 2014; Williams et al., 2010).

The MRN complex is among the earliest respondents to DSBs and is required for the recruitment of other repair factors and efficient activation of ATM and ATR upon DNA damage (Berkovich et al., 2007; Deshpande et al., 2014; Duursma et al., 2013; Lee and Paull, 2005; Mimitou and Symington, 2008). The involvement of the MRN complex in HR repair largely occurs through end resection of DSBs, which occurs in an MRE11 nuclease activity-dependent manner. Additionally, MRE11, which possesses endonuclease activity and 3′-5′ exonuclease activity, is the central factor of the MRN complex (Deshpande et al., 2016; Paull, 2018; Paull and Gellert, 1998; Trujillo et al., 1998). In S/G2 phase, MRE11 endonucleolytically cleaves the 5′ strand at DNA DSB ends and subsequently generates a single-stranded DNA gap via 3′ to 5′ exonucleolytic degradation (Paull, 2018; Wang et al., 2017). Importantly, this process prevents NHEJ and creates entry sites for EXO1- and DNA2-mediated 5′ to 3′ long-range resection, which is required for single-strand invasion and recombination (Anand et al., 2016; Cannavo and Cejka, 2014; Levikova et al., 2017; Paull, 2018; Reginato et al., 2017; Wang et al., 2017).

MRE11 deletion or mutation resulting in the loss of nuclease activity causes early embryonic lethality in mice and nonviability in cultured vertebrate cells (Buis et al., 2008; Hoa et al., 2016; Yamaguchi-Iwai et al., 1998). Furthermore, inherited hypomorphic mutations in MRE11 cause ataxia telangiectasia-like disorder (ATLD), a rare disease characterized by progressive cerebellar ataxia, developmental defects, immunodeficiency, and cancer predisposition (Stewart et al., 1999; Taylor et al., 2004). At the

A

MRE11 purification

Protein	# unique peptides	Coverage(%)
MRE11	64	70.6
RAD50	27	25.3
NBS1	17	24.8
C1QBP	11	62.8
RPA1	16	34.9
RPA2	6	30.7
RPA3	2	22.3
FXR1	2	4
PCNA	1	5

RAD50 purification

Protein	# unique peptides	Coverage(%)
RAD50	207	89.9
MRE11	66	68.9
NBS1	7	14.7
C1QBP	1	9.6

NBS1 purification

Protein	# unique peptides	Coverage(%)
NBS1	48	49.1
RAD50	143	69.1
MRE11	13	18.1
C1QBP	-	-

B

C1QBP purification

Protein	# unique peptides	Coverage(%)
C1QBP	9	36.9
YBX1	11	50
FXR2	37	67.6
FXR1	25	52.7
FMR1	28	49.5
RECQ4	14	18
MRE11	4	10.6
RAD50	10	10.6

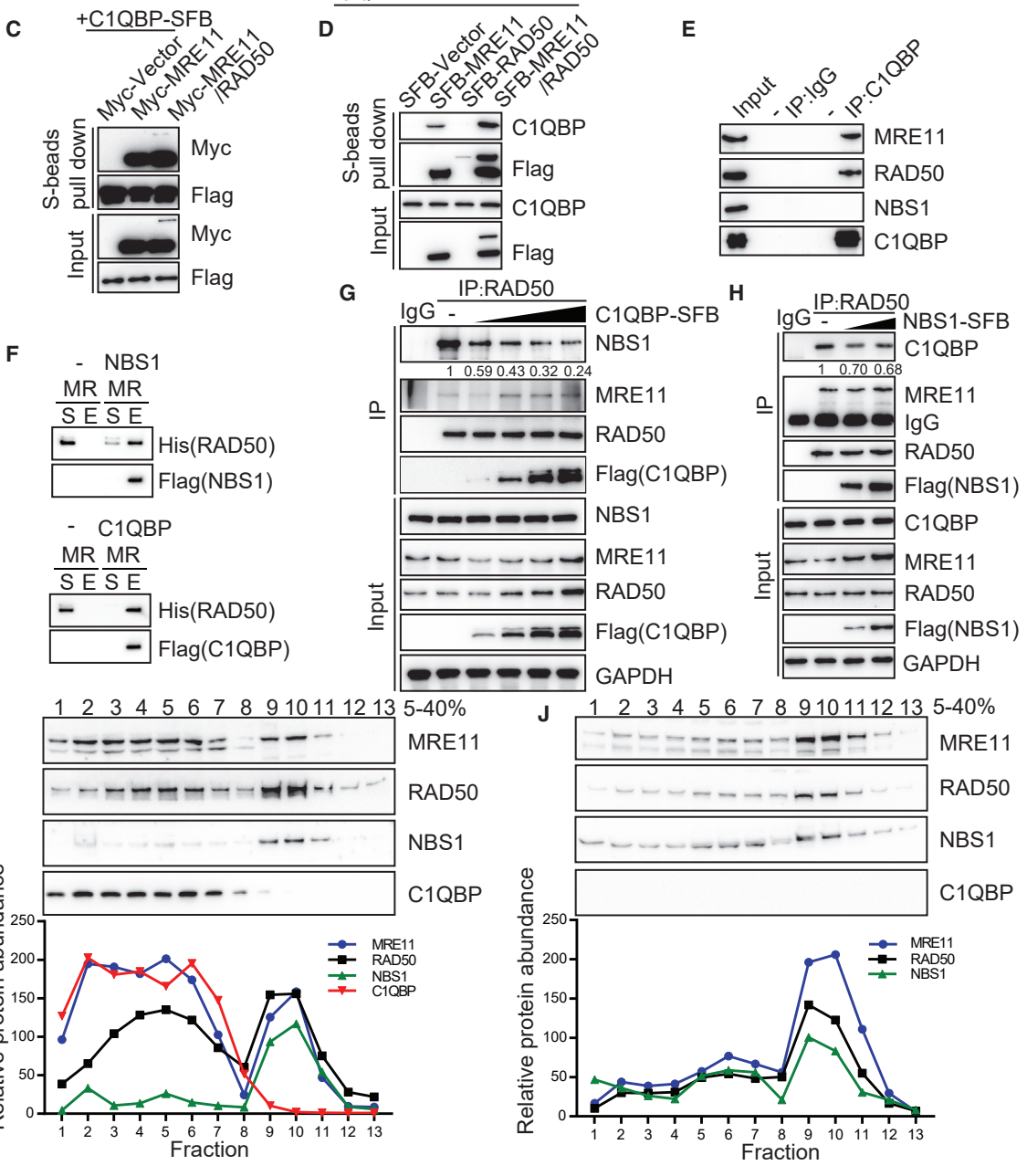

(legend on next page)

cellular level, depletion of MRE11 results in an increase in chromosomal aberrations and hypersensitivity to ionizing radiation (IR) or other DNA-damaging agents (Assenmacher and Hopfner, 2004). Additionally, mutations in the NBS1 cause Nijmegen breakage syndrome (NBS), which is clinically characterized by microcephaly, short stature, intellectual disability, immunodeficiency, radiation sensitivity, and an increased risk of cancer (Carney et al., 1998; Matsuura et al., 1998).

The MRE11 protein contains N-terminal phosphoesterase motifs that are essential for its nuclease activity and two DNA-binding motifs that endow it with intrinsic DNA-binding activity. MRE11 interacts with RAD50 at multiple interfaces and interacts with NBS1 at its phosphoesterase motif. MRE11 and RAD50 form stable MRE11/RAD50 (MR) complexes both *in vivo* and *in vitro* and constitute core catalytic components (Dolganov et al., 1996; Haber, 1998). The nuclease activities of MRE11 are stimulated by the binding of RAD50, which contains a coiled-coil domain for MRE11 binding and ATP hydrolytic activity to induce conformational change of the MRE11/RAD50 complex (Deshpande et al., 2017; Herdendorf et al., 2011; Lammens et al., 2011; Trujillo et al., 1998). Additionally, RAD50 is required for MRE11-mediated nuclease activity at double-stranded DNA. NBS1 regulates the catalytic activities of MRE11/RAD50 by promoting the endonuclease activity of MRE11 and stimulating RAD50-mediated ATP hydrolysis at DNA ends (Deshpande et al., 2016; Paull and Gellert, 1999; Schiller et al., 2012). NBS1 determines the outcomes of MRE11 nuclease activity by restraining its 3′-5′ exonuclease activity at open DNA ends while promoting its endo-/exonuclease activity at blocked DNA ends (Deshpande et al., 2016). Moreover, phosphorylated CtIP functions as a co-factor of the MRN endonuclease (Anand et al., 2016; Cannavo and Cejka, 2014).

MRE11 and RAD50 are highly evolutionarily conserved, whereas NBS1 and its homologs are found only in eukaryotes and are less conserved. Although knockdown of either MRE11 or RAD50 destabilizes all three MRN proteins, depletion of NBS1 has no effect on the level of either MRE11 or RAD50 protein (Zhong et al., 2007). Hence, it is not surprising that in addition to MRN complex formation, MRE11 and RAD50 can associate independently of NBS1. However, it remains unknown which co-factor can stabilize MRE11/RAD50.

Despite intensive investigation of the biology and biochemistry of the MRN complex, it is unclear how MRN is dynamically regulated. Surprisingly, in this study, we found that MRE11/RAD50 forms an MRC complex with C1QBP *in vivo* and *in vitro*. Our data indicate that C1QBP association with MRE11 is required to maintain a certain amount of MRE11 to prepare to repair damaged DNA and prevent MRE11 association with chromatin while limiting its enzymatic activity under normal conditions. In response to DNA damage, the ATM-mediated phosphorylation of MRE11-S676/S678 causes the dissociation of the MRC complex and the release of MRE11/RAD50 to initiate DNA end resection. The inhibition of C1QBP enhances the regression of tumors by chemotherapy. Taken together, our findings revealed that C1QBP is an important player in the DNA damage response and suggests that C1QBP may serve as a therapeutic target for cancer treatments.

RESULTS

C1QBP Is a Binding Partner of MRE11 and RAD50

To identify regulatory factors of the MRN complex, proteins associated with MRE11, RAD50, and NBS1 were purified by tandem affinity purification (TAP) and analyzed by mass spectrometry (MS) (Figures 1A and S1A; Tables S1, S2, and S3). As expected, MRE11/RAD50/NBS1 formed a tightly trimeric complex *in vivo* (Figures 1A and S1A). Surprisingly, complement component 1q subcomponent binding protein (C1QBP) was one of the strongest binding partners of MRE11 but in the absence of NBS1 binding proteins (Figure 1A). Reciprocal TAP-MS showed that MRE11 and RAD50, but not NBS1, copurified with C1QBP (Figure 1B; Table S4).

C1QBP is an evolutionarily conserved protein and has been reported to be involved in immune response, apoptosis, oxidative phosphorylation, transcription, mitochondrial translation, and pre-mRNA splicing (Ghebrehiwet and Peerschke, 2004; Itahana and Zhang, 2008; Jiang et al., 1999; Xu et al., 2009; Yagi et al., 2012). C1QBP is a multicompartmental cellular protein that distributes in mitochondria, plasma membrane, cytosol, and nucleus (Ghebrehiwet and Peerschke, 2004) (Figure S1B). To confirm that C1QBP interacts with MRE11, coimmunoprecipitation and GST pull-down assays were performed. The interaction between *in vitro* purified GST-C1QBP and mammalian cells expressing MRE11 was assessed (Figure S1C). Overexpressed or endogenous C1QBP copurified with MRE11 in both cytoplasm and nucleus (Figures 1C, 1D, and S1D), and endogenous C1QBP also associated with endogenous MRE11 and RAD50, but not with NBS1 (Figure 1E). To further explore whether MRE11/RAD50 directly interacts with C1QBP, we purified C1QBP-Flag from *Escherichia coli* and the MRE11/ RAD50-His

Figure 1. C1QBP Interacts with MRE11 and RAD50

(A and B) TAP-MS identifies MRE11-, RAD50-, NBS1- (A), or C1QBP (B)-associated proteins.

(C and D) Interaction between C1QBP and MRE11 in 293T cells.

(E) Endogenous C1QBP associates with MRE11 in 293T cells.

(F) C1QBP interacts with MRE11/RAD50 *in vitro*. C1QBP-Flag (74–282 aa) and MRE11/RAD50-His complex were expressed and purified from *E. coli* and yeast, respectively; 140 ng C1QBP-Flag was mixed with 470 ng of MRE11/RAD50 (MR) and then complexes were pulled down using anti-Flag M2 affinity gel. The supernatant (*S*) containing unbound proteins and the eluate (*E*) fractions were analyzed by western blotting using the indicated antibodies.

(G and H) Increasing expression of C1QBP disrupted the MRE11/RAD50 and NBS1 interaction (G) and increasing expression of NBS1 disrupted the MRE11/RAD50 and C1QBP interaction (H) in 293T cells. The blots of immunoprecipitated NBS1 and C1QBP were quantified and normalized by comparing with immunoprecipitated RAD50.

(I and J) Fractions of wild type (I) or C1QBP-knockout (J) HeLa cells were separated by sucrose gradient centrifugation. The amounts of the indicated proteins were quantified using ImageJ.

See also Figure S1 and Tables S1, S2, S3, and S4.

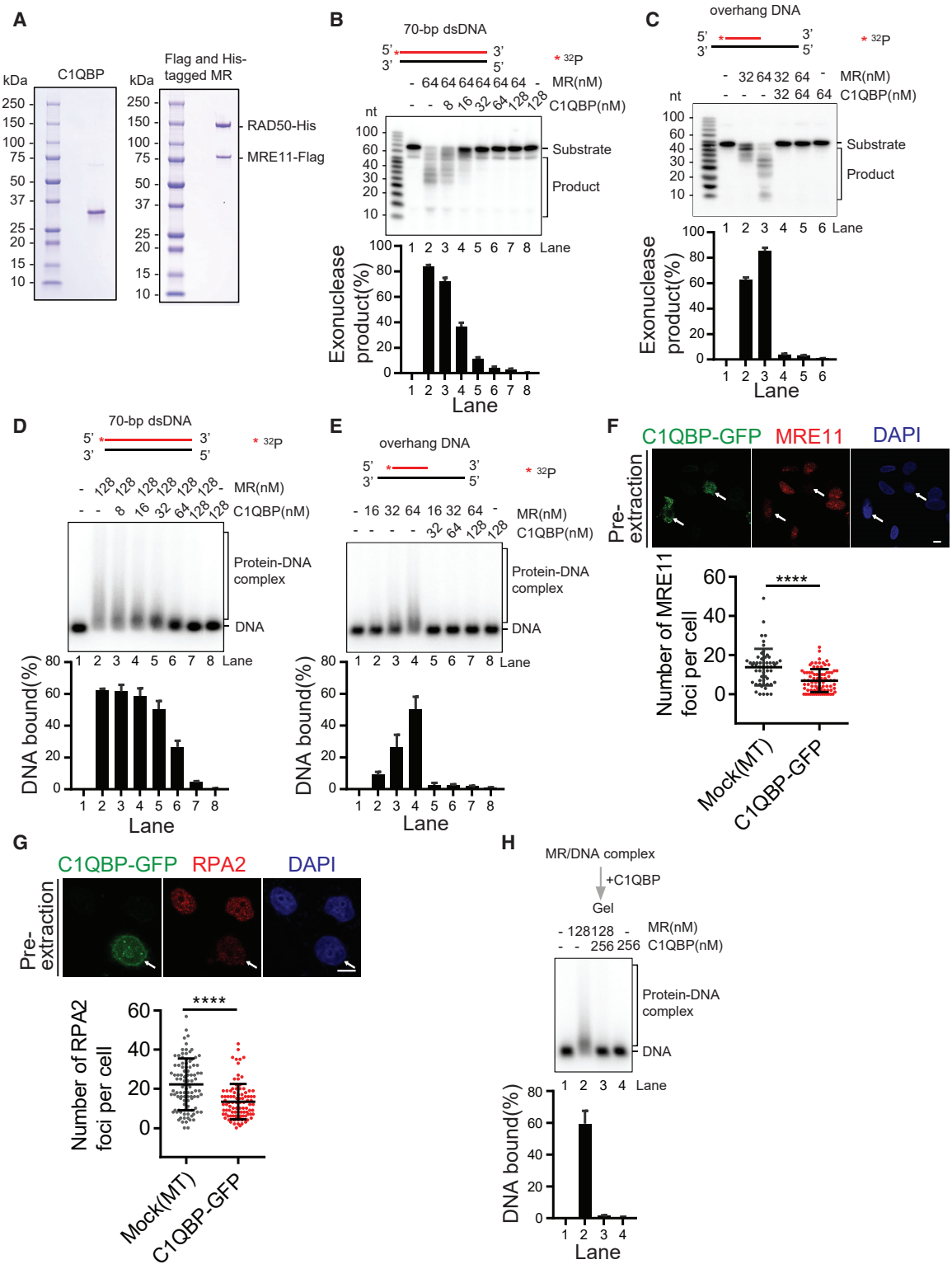

Figure 2. C1QBP Prevents MRE11 DNA Binding and Exonuclease Activity

(A) Expression and purification of C1QBP and MRE11/RAD50 (MR) proteins *in vitro*. Flag-tagged MRE11 and His-tagged RAD50 were coexpressed and purified from yeast, and Flag-tagged C1QBP (74–282 aa) was purified from *E. coli*.

(B and C) C1QBP inhibits the exonuclease activity of MRE11. The data are presented as means ± SD.

(legend continued on next page)

complex from yeast (Figures S1E and S1F), and an *in vitro* pull-down assay showed that, in addition to the MRN complex, MRE11/RAD50 efficiently formed a complex with C1QBP (MRC complex) (Figure 1F).

Notably, increasing C1QBP expression disrupted the interaction between MRE11/RAD50 and NBS1 in total fraction and nucleus fraction (Figures 1G and S1G), and increasing that of NBS1 also disrupted the interaction between MRE11/RAD50 and C1QBP (Figure 1H), suggesting that MRC and MRN are independent and mutually exclusive complexes *in vivo*. Moreover, a sucrose gradient fraction of HeLa cell extracts showed that most MRE11/RAD50 cosedimented with NBS1 but that a substantial portion of MRE11/RAD50 cosedimented with C1QBP (Figure 1I). Interestingly, C1QBP and NBS1 were almost in a completely different fraction (Figure 1I), also indicating that MRN and MRC are mutually exclusive. Surprisingly, when cells were deleted of C1QBP, the presence of MRE11/RAD50 in the small-molecular-weight fraction was dramatically reduced and predominantly comigrated with NBS1 in the large-molecular-weight fraction (Figure 1J). Accordingly, deletion of C1QBP promoted MRN complex formation in the nucleus (Figure S1H). In contrast, we found that CtIP, the best characterized licensing factor for MRE11-mediated resection, did not interact with C1QBP and had no effect on MRC complex formation (Figures S1I and S1J). Together, these data strongly suggest that, in addition to the MRE11/RAD50/NBS1 complex, an MRE11/RAD50/C1QBP (MRC) complex exists both *in vivo* and *in vitro*.

C1QBP Inhibits MRE11 Exonuclease Activity by Preventing Its DNA Binding

Because MRE11/RAD50 possesses 3′-5′ exonuclease activity *in vivo* and *in vitro*, we next evaluated whether C1QBP regulates the enzymatic activity of MRE11. MRE11/RAD50 complex was expressed and purified from yeast, and C1QBP proteins were purified from *E. coli* (Figure 2A). We confirmed that purified MRE11/RAD50 efficiently catalyzed 3′ to 5′ exonucleolytic degradation of different substrates *in vitro*, including blunt-end dsDNA and dsDNA with 3′ and 5′ overhangs (Figures 2B, 2C, and S2A). Importantly, C1QBP significantly repressed MRE11/RAD50 exonucleolytic digestion of dsDNA substrates (Figures 2B and 2C).

We then investigated the molecular mechanism by which C1QBP inhibits the nuclease activity of MRE11 and addressed whether physical interaction between C1QBP and MRE11/RAD50 affects the DNA-binding ability of MRE11/RAD50. Electrophoretic mobility shift assays (EMSAs) showed that the MRE11/RAD50 complex alone bound to blunt-end dsDNA or dsDNA with overhangs with high affinity (Figures 2D and 2E). However, C1QBP almost completely disrupted the ability of MRE11/RAD50 to bind dsDNA (Figures 2D–2E).

Upon DSB occurrence, MRE11 recruitment to these sites is the earliest event and is required for efficient DDR. We observed that C1QBP overexpression reduced the formation of MRE11 foci and had no effect on the cell-cycle distribution (Figures 2F and S2B). Accordingly, C1QBP overexpression also inhibited RPA2 and RAD51 foci formation (Figures 2G and S2C) and ATR/CHK1 activation upon DNA damage (Figure S2D), suggesting that excessive C1QBP inhibits DNA end resection and DDR *in vivo*.

Interestingly, C1QBP could also interact with MRE11/RAD50 when already present in the MRE11/RAD50/DNA complex, suggesting that C1QBP can either form the MRE11/RAD50/DNA/C1QBP complex or displace DNA from the MRE11/RAD50/DNA complex (Figure S2E). We further revealed that C1QBP disrupted the existing MRE11/RAD50/DNA complex (Figure 2H); however, neither ssDNA nor dsDNA could disturb MRC complex formation (Figure S2F), suggesting that C1QBP binds MRE11/RAD50 with higher affinity and might help MRE11/RAD50 to dissociate from DNA upon completion of DNA resection. Consistently, C1QBP translocated to nucleus and was recruited to chromatin or laser-induced DNA damaged sites at late stage of DNA damage repair (Figures S2G–S2I), indicating that C1QBP could be recruited to DSBs to facilitate the dissociation of MRE11 with DNA upon completion of DNA repair.

These data clearly show that C1QBP inhibits MRE11 exonuclease activity and DNA end resection by preventing its DNA binding.

C1QBP Interacts with the GAR Motif of MRE11

To investigate the region responsible for MRE11 binding with C1QBP, serial deletion mutants of MRE11 were generated and transfected in cells stably expressing C1QBP-SFB (Figure 3A). Deletion of the GAR (glycine-arginine-rich) motif of MRE11 completely disrupted the interaction between MRE11 and C1QBP (Figure 3A) but had no effect on MRE11/RAD50 binding and increased MRE11/NBS1 binding (Figure 3B), indicating that the GAR domain is required for binding between MRE11 and C1QBP. Additionally, deletion of the second DNA-binding domain of MRE11 (MD5) increased the interaction between MRE11 and C1QBP (Figures 3A and S3A). TAP purification was performed using MRE11 with a deleted GAR motif; as expected, C1QBP was absent among the binding partners for the MRE11-ΔGAR mutant (Figure 3C; Tables S5 and S6). Importantly, we further identified that MRE11-R572Q and -R576Q, frequent GAR motif missense mutations among cancer patients with unknown reasons (Caminsky et al., 2016; Yadav et al., 2017), displayed dramatically reduced interaction with C1QBP, with no influence on the interaction with RAD50 (Figures 3D and S3B). However, the R570Q mutant of

(D and E) C1QBP prevents MRE11/RAD50 from associating with DNA. The data are presented as means ± SD.

(F and G) C1QBP overexpression represses MRE11 (F) and p-RPA2 (S4/S8) (G) foci formation. HeLa cells were transiently transfected with C1QBP-GFP and were synchronized at S phase, followed by treatment with CPT (1 μM) for 2 h. The cells were pre-extracted and were immunostained with the indicated antibodies. The data are presented as means ± SD (****$p < 0.0001$). Scale bar, 10 μm.

(H) C1QBP disrupts the association between MRE11/RAD50 (MR) and DNA. MRE11/RAD50 (128 nM) and dsDNA (4 nM) substrate were premixed and added with the indicated amount of C1QBP. After 15 min of incubation at 37°C, the reactions were subjected to electrophoresis; the gels were dried onto positively charged nylon membranes and subjected to phosphorimaging analysis. The data are presented as means ± SD.

See also Figure S2.

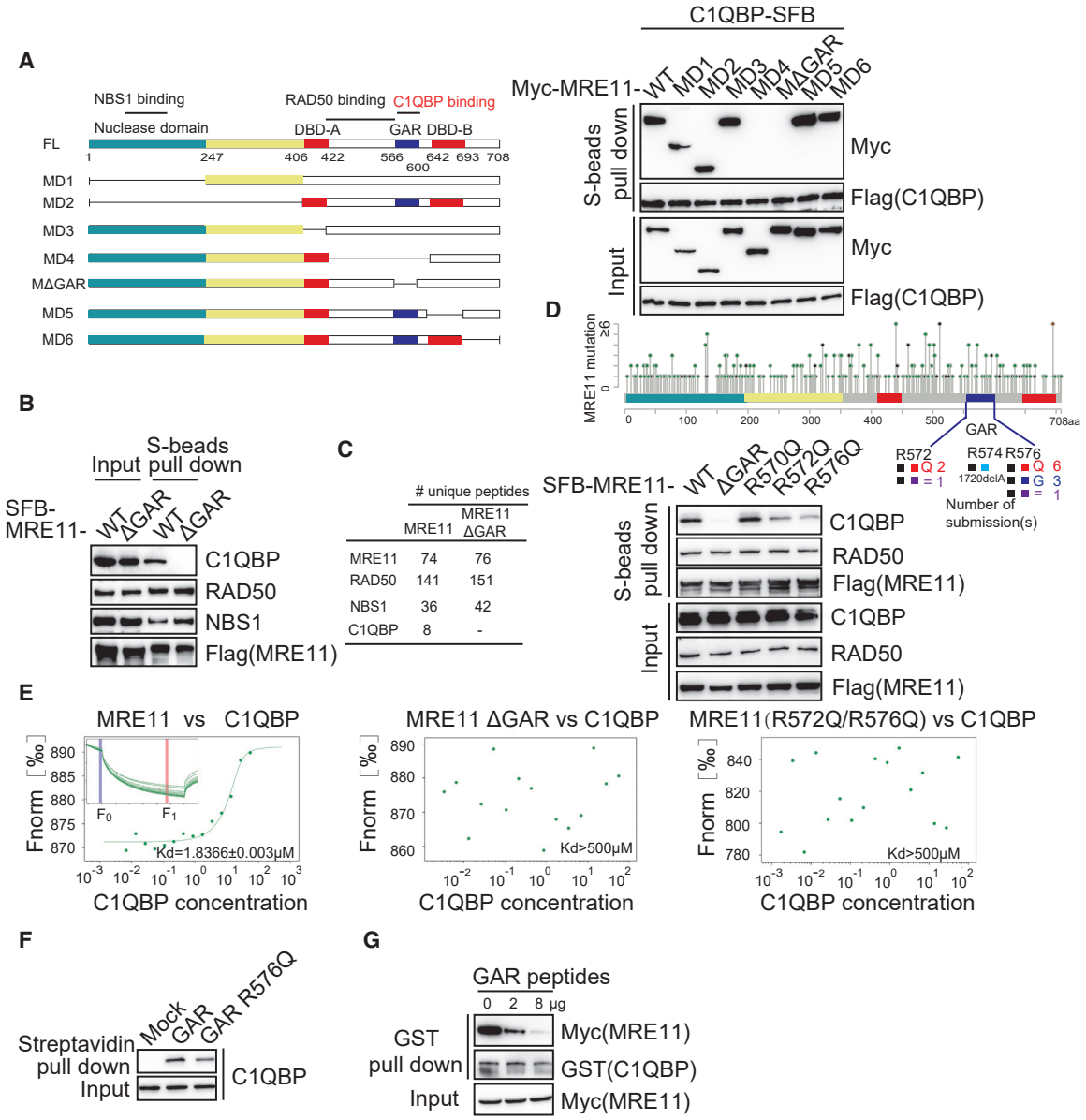

Figure 3. C1QBP Directly Binds to the GAR Domain of MRE11

(A) Mapping the MRE11 domain that is important for interaction with C1QBP.

(B) The MRE11-ΔGAR mutant only disrupts the interaction between MRE11/C1QBP but has no effect on the interaction between MRE11/RAD50.

(C) The GAR motif of MRE11 is required for MRE11/C1QBP interaction. 293T cells that stably expressed SFB-MRE11 or SFB-MRE11-ΔGAR were purified by tandem affinity purification and analyzed by mass spectrometry. The table provides summaries of the proteins identified by mass spectrometry.

(D) Mapping the residues of MRE11-GAR motif that are important for interaction with C1QBP. The MRE11 mutations in breast cancers and ATLD were obtained from c-BioPortal and ClinVar.

(E) Microscale thermophoresis (MST) assays showed that MRE11 and C1QBP interacted *in vitro* but that the MRE11-ΔGAR and MRE11-R572/576Q mutant showed disrupted interaction.

(F) Biotin-labeled MRE11-GAR or MRE11-GAR-R576Q peptides pulled down by *E. coli*-expressed GST-C1QBP using streptavidin agarose.

(G) MRE11-GAR peptides disrupt the MRE11/C1QBP interaction.

See also Figure S3 and Tables S5 and S6.

MRE11, next to R572/R576 but with no identified mutation in patients, had no effect on MRE11/C1QBP interaction. Moreover, the R572Q/R576Q double mutant of MRE11 completely disrupted the interaction between MRE11 and C1QBP (Figure S3B). We further confirmed these interactions using the microscale thermophoresis (MST) assay. As shown in Figure 3E, compared with wild type MRE11, the MRE11-ΔGAR or an MRE11-R572/576Q mutant exhibited no interaction with

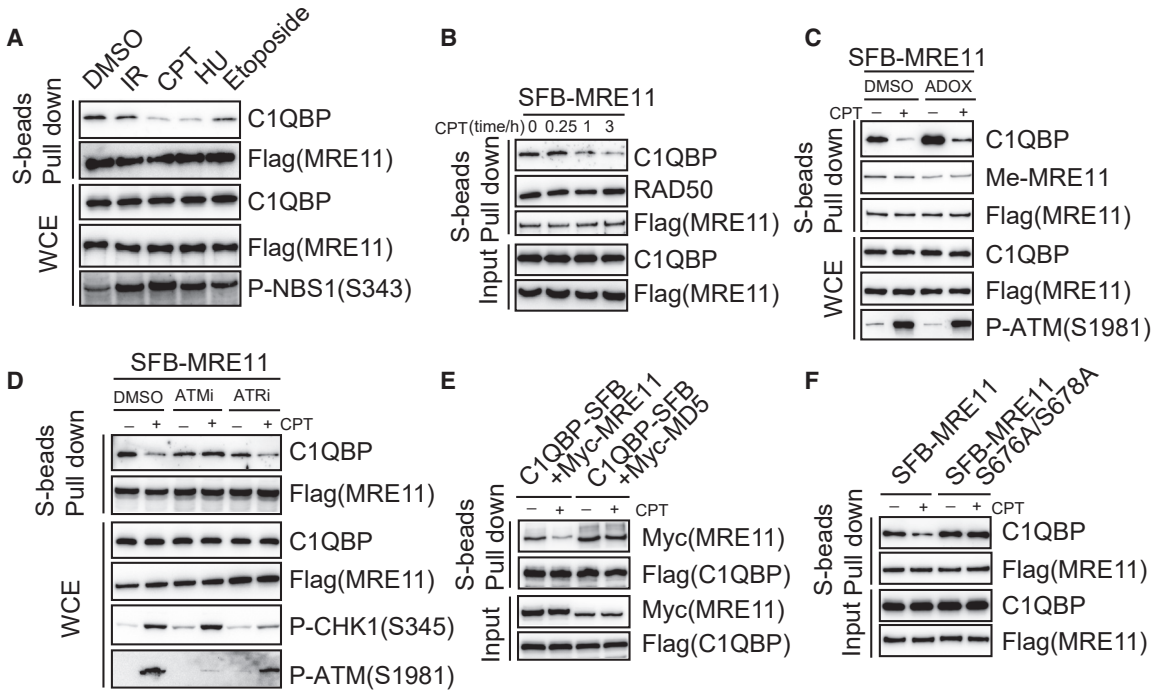

Figure 4. DNA Damage-Induced MRE11 Phosphorylation Dissociates the MRC Complex

(A) The C1QBP/MRE11 interaction is disrupted by DNA damage treatments. 293T cells stably expressing SFB-MRE11 were treated with CPT (1 μM, 3 h), IR (10 Gy, 5 h), etoposide (50 μM, 8 h), or HU (1 mM, 8 h), and cell lysates were pulled down by S protein-Sepharose and immunoblotted with the indicated antibodies.

(B) The CPT-induced dissociation between C1QBP/MRE11 is time-dependent.

(C) Adox treatment increased the interaction between C1QBP/MRE11 but had no effect on DNA damage-induced dissociation of C1QBP/MRE11. 293T cells transfected with SFB-MRE11 were treated with DMSO or methyltransferase inhibitor Adox (10 μM) for 15 h and were further treated with or without CPT (1 μM) for 2 h. Me-MRE11 is detected by anti-dimethyl-arginine asymmetric (ASYM25) antibody.

(D) ATM inhibitor abolishes DNA damage-induced dissociation of C1QBP/MRE11. SFB-MRE11 stable cells were pretreated with ATR inhibitor (VE-821, 10 μM) or ATM inhibitor (KU55933, 10 μM) for 12 h and then were further treated with or without CPT (1 μM) for 2 h.

(E) The second DNA-binding domain deletion mutant of MRE11 (MD5) represses the DNA damage-induced dissociation of C1QBP/MRE11.

(F) The S676A/S678A mutant of MRE11 represses DNA damage-induced dissociation of C1QBP/MRE11.

See also Figure S4.

C1QBP. Importantly, the GAR peptide was sufficient to interact with C1QBP *in vitro*, but clearly decreased interaction was observed with GAR-R576Q (Figure 3F). Furthermore, the GAR peptides of MRE11 significantly disrupted the MRE11/C1QBP interaction by competing with MRE11 for binding C1QBP (Figure 3G). These data clearly show that the GAR domain, especially the R572 and R576 residues, of MRE11 is crucial to mediate the interaction with C1QBP.

DNA Damage-Induced MRE11 Phosphorylation Dissociates the MRC Complex

It has been reported that MRE11 and NBS1 interaction is induced upon DNA damage (Chang et al., 2016; Wu et al., 2012; Zhou et al., 2017) (Figure S4A). Next, we evaluated the interactions between MRE11 and C1QBP upon DNA damage. Interestingly, interaction between C1QBP and MRE11 was significantly reduced upon DNA damage, including that induced by camptothecin (CPT), ionizing radiation (IR), hydroxyurea (HU), and etoposide (Figure 4A), and this DNA damage-induced dissociation between MRE11 and C1QBP was time- and dose-dependent (Figures 4B, S4B, and S4C).

Next, we explored possible upstream signals of DNA damage-induced dissociation of the MRC complex. C1QBP directly interacts with the GAR motif of MRE11, which has been reported to be a PRMT1-mediated methylated motif that is crucial for DNA damage checkpoint control (Boisvert et al., 2005; Yu et al., 2012). Additionally, methylation of the GAR motif is inhibited by the broad-spectrum methyltransferase inhibitor adenosine dialdehyde (Adox) (Boisvert et al., 2005; Yu et al., 2012). Interestingly, Adox failed to block DNA damage-induced dissociation of MRE11 and C1QBP (Figure 4C), although the interaction between MRE11 and C1QBP increased dramatically, and the interaction between MRE11 and NBS1 decreased clearly following treatment of cells with Adox (Figures 4C and S4D). This result suggests that the methylation of MRE11 might inhibit the interaction between MRE11 and C1QBP, but this process is not regulated by DNA damage. Next, we found that an ATM inhibitor, but not an ATR inhibitor, completely disrupted DNA damage-induced dissociation of MRE11/C1QBP (Figure 4D), suggesting that ATM-mediated phosphorylation is required for disruption of the MRC complex upon DNA damage. Interestingly, at late stage of DNA damage repair, the ATM phosphorylation level

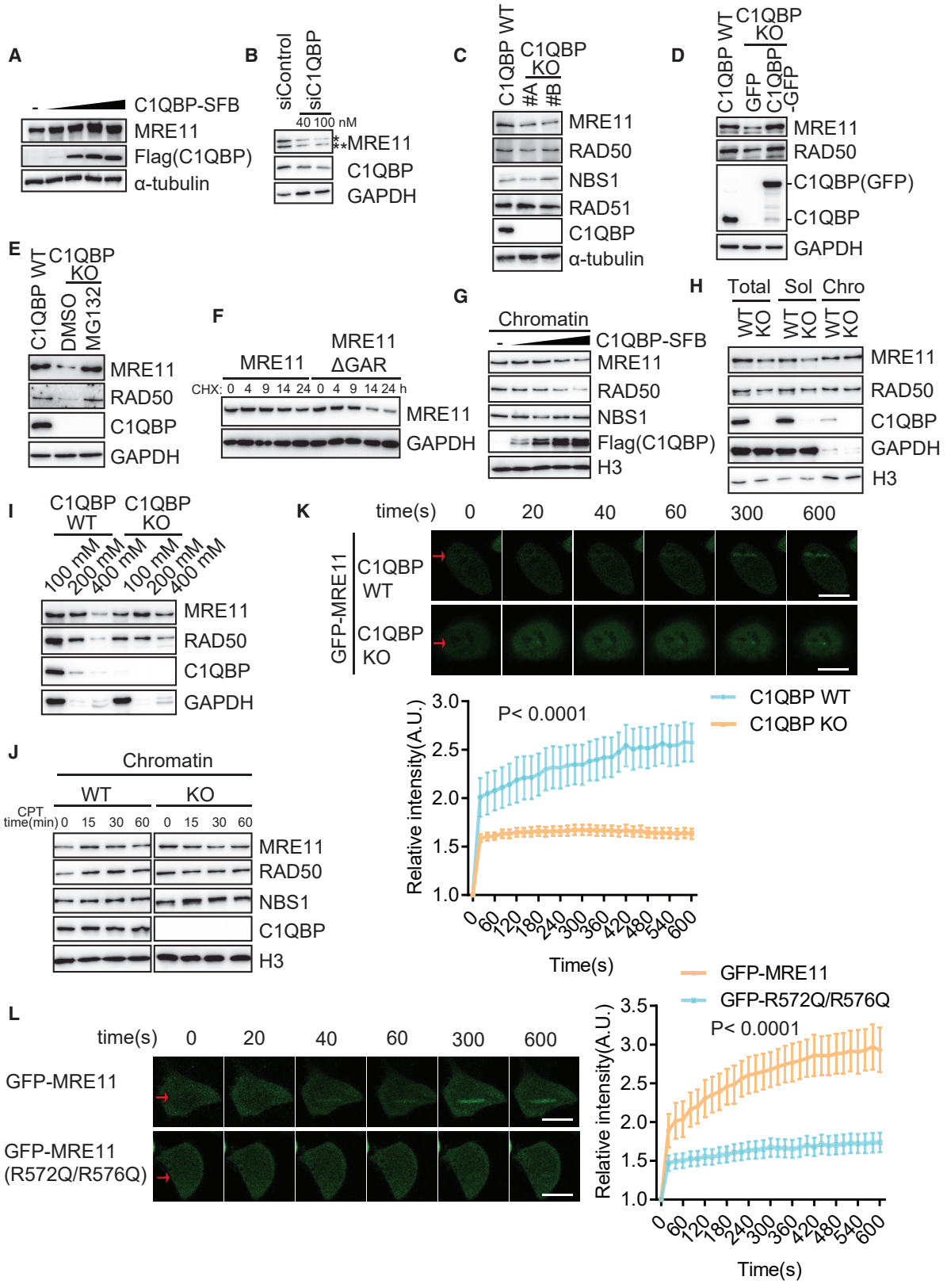

(legend on next page)

decreased while the interaction between C1QBP and MRE11 increased (Figure S4E), suggesting that MRE11 forms inactive MRC complex again upon completion of DNA repair.

It was reported that S150 of C1QBP is a substrate of ATM (Itahana and Zhang, 2008). However, we found that the C1QBP S150A mutant has no effect on the dissociation between MRE11 and C1QBP upon DNA damage (Figure S4F). Additionally, by mass spectrometry, we failed to identify S150 of C1QBP to be phosphorylated under normal conditions and upon DNA damage treatment (Figure S4G). Our previous data showed that deletion of the second DNA-binding domain of MRE11 (MD5) increased the interaction between MRE11 and C1QBP (Figures 3A and S3A). Therefore, we further evaluated whether MD5 of MRE11 affected the dissociation between MRE11 and C1QBP upon DNA damage. As a result, MRE11 loss of the second DNA-binding domain repressed the dissociation between MRE11 and C1QBP upon DNA damage (Figure 4E). Furthermore, it has been reported that MRE11 is also phosphorylated by ATM at S676 and S678 in response to agents that induce DNA DSBs (Kijas et al., 2015; Matsuoka et al., 2007). Interestingly, S676 and S678 are among the second DNA binding domain of MRE11 and phosphosite mutant MRE11-S676A/S678A totally abolished the dissociation between MRE11 and C1QBP upon DNA damage (Figure 4F). These data clearly show that ATM-mediated MRE11 S676/S678 phosphorylation causes dissociation of the MRC complex upon DNA damage.

C1QBP Stabilizes MRE11/RAD50 and Prevents MRE11/RAD50 Chromatin Association

Notably, the protein level of endogenous MRE11 or stably expressed MRE11 was increased dramatically in cells overexpressing C1QBP, suggesting that C1QBP may stabilize MRE11/RAD50 (Figures 5A and S5A). A decrease in both endogenous and exogenous MRE11 protein levels was observed in 293T cells when C1QBP was depleted with small interfering RNA (siRNA) (Figure 5B). We further generated C1QBP-knockout HeLa and A375 cell lines, as confirmed by genomic sequencing (Figure S5B) and found that C1QBP knockout clearly reduced MRE11 and RAD50 protein levels but had only a mild effect on NBS1 protein levels (Figures 5C and S5C). Importantly, the MRE11 and RAD50 protein level was rescued in C1QBP-knockout cells by reconstituting C1QBP expression (Figure 5D). Moreover, neither the mRNA level of MRE11 nor the distribution of cell cycle changed upon C1QBP deletion (Figures S5D and S5E), indicating that C1QBP does not regulate MRE11 expression by affecting transcription or the cell cycle. The proteasome inhibitor MG132 also rescued MRE11 and RAD50 protein expression in C1QBP-knockout cells (Figure 5E), suggesting that C1QBP stabilizes MRE11 by preventing proteasome-mediated MRE11 degradation. It should be noted that the half-life of the MRE11-ΔGAR mutant, which cannot bind to C1QBP, was significantly shorter than that of wild type MRE11 (Figure 5F).

Our previous data showed that C1QBP inhibits MRE11 exonuclease activity by preventing its DNA binding *in vitro* (Figure 2). We further found that the overexpression of C1QBP dramatically decreased the protein retention of MRE11/RAD50 in the chromatin fraction (Figure 5G), indicating that C1QBP could also prevent MRE11 chromatin association *in vivo*. Next, the relative amounts of soluble and chromatin MRE11/RAD50 were quantified in C1QBP wild type and knockout cells, revealing that the proportion of MRE11/RAD50 in the chromatin fraction of C1QBP-depleted cells was significantly increased (Figure 5H). Moreover, in C1QBP-knockout cells, MRE11 associated with chromatin more tightly (400 mM NaCl fraction) even without DNA damage treatment (Figure 5I), indicating that the loss of C1QBP promotes the association of MRE11 with undamaged chromatin.

We further compared the recruitment of MRE11 to chromatin in wild type cells and C1QBP-deleted cells upon DNA damage. In the former, the level of MRE11/RAD50 protein in the chromatin fraction clearly increased upon CPT treatment; with the loss of C1QBP, the level of MRE11/RAD50 protein in the chromatin fraction was not clearly altered upon DNA damage treatment (Figure 5J). Accordingly, deletion of C1QBP retarded laser-induced damage recruitment of GFP-MRE11 (Figure 5K). Moreover, the MRE11-R572Q/R576Q mutant, which cannot bind to C1QBP, was recruited to DNA damage sites slower than wild type MRE11 (Figure 5L). These data suggest that, although excess levels of C1QBP impaired MRE11 foci formation by preventing DNA binding by MRE11 (Figure 2G), insufficient C1QBP also

Figure 5. C1QBP Stabilizes MRE11/RAD50 *In Vivo*

(A) C1QBP stabilizes MRE11 in a dose-dependent manner in 293T cells.

(B) Transient knockdown of C1QBP decreased both the endogenous and exogenous MRE11 protein levels. **, represents endogenous MRE11; *, represents stably expressed SFB-MRE11.

(C) Knockout of C1QBP decreases MRE11 protein levels.

(D) Reconstitution of C1QBP expression restores MRE11 expression in C1QBP-knockout cells.

(E) MG132 rescues the C1QBP deletion-induced decrease in the MRE11 protein.

(F) The MRE11-ΔGAR mutant is unstable *in vivo*. C1QBP stable cells transiently expressing wild type or the ΔGAR mutant of MRE11 were treated with 10 μg/mL of cycloheximide (CHX) for the indicated time. Western blotting was carried out using the indicated antibodies.

(G) Overexpression of C1QBP reduces MRE11 chromatin loading.

(H) Deletion of C1QBP increases MRE11 chromatin loading.

(I) Proteins were sequentially extracted from wild type or C1QBP knockout HeLa cells by increasing the amount of salt (NETN buffer contains 100/200/400 mM NaCl). The amount of MRE11 present in each fraction was measured by immunoblotting.

(J) Wild type HeLa cells and C1QBP-knockout cells were transfected with the empty C-SFB vector or C1QBP-SFB for 48 h and were treated with CPT (1 μM) for the indicated time. The chromatin fraction was extracted and immunoblotted with the indicated antibodies.

(K) Deletion of C1QBP retards the recruitment of MRE11 to DSBs. The data are presented as means ± SEM ($n \geq 10$). Scale bar, 10 μm.

(L) The MRE11-R572Q/R576Q mutant was recruited to DNA damage sites slower than the wild type MRE11. The data are presented as means ± SEM ($n = 10$). Scale bar, 10 μm.

See also Figure S5.

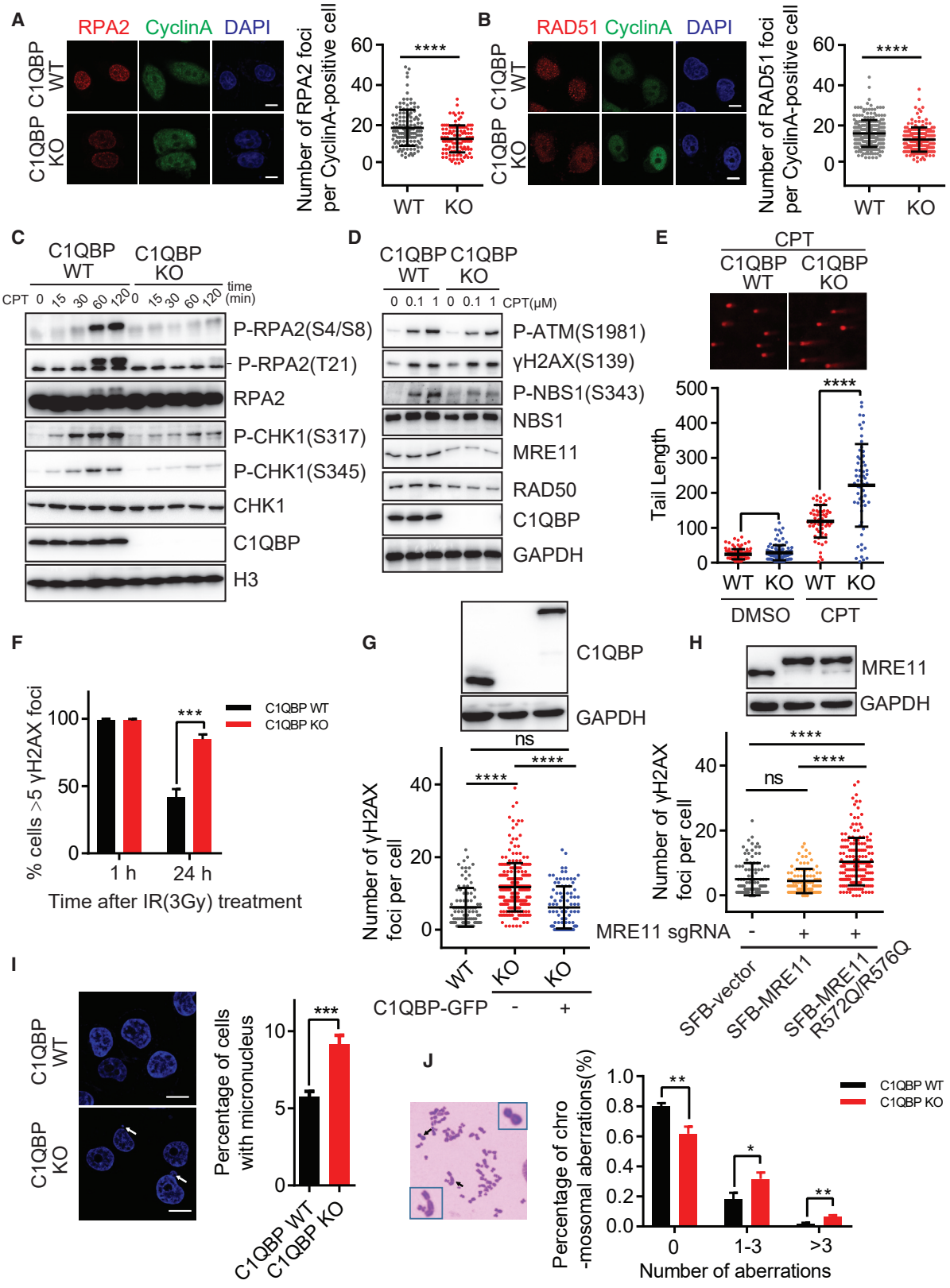

(legend on next page)

impaired recruitment of MRE11 to DNA damage sites by increasing nonspecific associations of MRE11 with undamaged chromatin (Figure 5K).

Together, these data show that C1QBP maintains the MRE11 protein pool to prepare to repair damaged DNA but prevents the association of MRE11 with undamaged chromatin.

C1QBP Is Essential to Maintain Genomic Stability by Promoting Efficient DDR

MRE11 is the central nuclease component of the MRN complex that processes resection of DNA ends, a function that is crucial for the formation of single-stranded DNA (ssDNA) and initiating HR. We found that C1QBP depletion significantly reduced RPA2 and Rad51 foci formation and DNA fiber length (Figures 6A, 6B, and S6), indicating defects in DNA end resection and the formation of ssDNA at DNA DSBs in C1QBP-deficient cells. MRE11 is also the central player in activating multiple checkpoint pathways, including ATM and ATR pathways. Therefore, we assessed whether C1QBP is required for MRE11-mediated DDR. Indeed, we observed severely impaired ATR and ATM activation in C1QBP-deficient cells (Figures 6C and 6D), suggesting that C1QBP is crucial for efficient DDR after DNA damage.

Furthermore, C1QBP-deficient cells failed to efficiently repair CPT- or IR-induced DNA damage (Figures 6E and 6F), suggesting that the loss of C1QBP impairs DNA repair capability. Importantly, C1QBP reconstitution rescued the DNA repair capacity in C1QBP-knockout cells (Figure 6G). Moreover, wild type MRE11, but not the MRE11 R572Q/R567Q mutant with loss of C1QBP-binding ability, restored the DNA repair capacity of MRE11-depleted cells (Figure 6H). These data indicate that the interaction between MRE11 and C1QBP is crucial for efficient DNA repair. MRE11 is the pivotal nuclease required to maintain genomic stability and chromosome integrity. In our study, C1QBP-depleted cells exhibited significantly increased spontaneous formation of micronuclei (Figure 6I) and spontaneous chromosome breaks (Figure 6J), suggesting that C1QBP is required to maintain genomic stability and that the loss of C1QBP elevates cancer risk.

Taken together, these data clearly show that C1QBP is essential to maintain genomic stability by promoting efficient DDR and DNA repair.

C1QBP Is a Potential Therapeutic Target for Cancer Treatment

It was reported that MRE11 and many DNA repair factors are overexpressed in breast cancer to maintain cancer cell genomic stability and promote radiotherapy and chemotherapy resistance via enhanced DNA repair activity. The results of this study provide evidence that C1QBP stabilizes the MRE11 protein and regulates MRE11 at multiple levels. To further determine the pathological relevance of C1QBP and MRE11, we performed immunohistochemical staining of C1QBP and MRE11 using a breast cancer tissue microarray (Figure 7A). Notably, upregulation of C1QBP and MRE11 was observed in 76.6% (92 of 120) and 80.8% (97 of 120) of breast tumors, whereas only 25.6% (10 of 39) and 28.2% (11 of 39) of normal mammary tissues exhibited high expression of C1QBP and MRE11, respectively (Figure 7A). Importantly, we also observed a significant positive correlation between C1QBP and MRE11 in the breast carcinomas tested, whereby 85.9% (79 of 92) of breast tumors with high C1QBP expression also showed high MRE11 levels (Figure 7A).

Moreover, according to the Kaplan-Meier plot database, high expression of both C1QBP and MRE11 was associated with a worse overall survival in breast cancer (Figure 7B). Furthermore, high C1QBP expression was related to a poor prognosis in ovarian cancer patients treated with conventional chemotherapy by a DNA topoisomerase I inhibitor (Topotecan) (Figure 7C). Thus, we propose that C1QBP is a potential therapeutic target for cancer treatment.

Next, we found that C1QBP-knockout cells displayed hypersensitivity to DNA damage by the topoisomerase I inhibitor CPT, IR, and olaparib (Figure 7D), and the sensitivity could be rescued by the reconstitutions of C1QBP. Camptothecin-11 (CPT-11) also dramatically suppressed C1QBP-deletion melanoma A375 cell xenograft tumor growth but had less of an effect on wild type A375 cell xenograft tumor growth (Figure 7E). These data suggest a potential role for C1QBP as a therapeutic target for cancer treatment.

DISCUSSION

The MRE11 nuclease has been intensively investigated because of its central role in maintaining genomic stability and controlling

Figure 6. C1QBP Is Essential for MRE11 Recruitment to DSBs and Efficient DDR

(A and B) Loss of C1QBP represses p-RPA2 (S4/S8) (A) and RAD51 (B) foci formation. The data are presented as means ± SD (****$p < 0.0001$). Scale bar, 10 μm.

(C) C1QBP is required for efficient ATR-CHK1 activation upon DNA damage. C1QBP-wild type cells and C1QBP-knockout cells were treated with CPT (1 μM) for the indicated time, and cell lysates were immunoblotted with the indicated antibodies.

(D) C1QBP is required for efficient ATM activation upon DNA damage.

(E) The DNA repair capability is repressed in C1QBP-knockout cells. C1QBP-wild type cells and C1QBP-knockout HeLa cells were arrested in S phase and treated with 1 μM CPT for 2 h. After incubation for 24 h, the cells were analyzed by the comet assay. The data are presented as means ± SD (****$p < 0.0001$, ns: no significance).

(F) Loss of C1QBP inhibits the removal of γ-H2AX foci. The data are presented as means ± SD (***$p < 0.001$).

(G) The reconstitution of stably expressed C1QBP rescued DNA repair capacity in C1QBP-knockout cell. The data are presented as means ± SD (****$p < 0.0001$, ns: no significance).

(H) The R572Q/R567Q mutant of MRE11 fails to restore the DNA repair capacity of MRE11-depleted cells. The data are presented as means ± SD (****$p < 0.0001$, ns: no significance).

(I) Loss of C1QBP increases genomic instability. DAPI staining of C1QBP-wild type and C1QBP-knockout A375 cells was performed, and micronuclei were counted in over 1,000 cells each. Data are presented as means ± SD ($n = 3$, ***$p < 0.001$). Scale bar, 10 μm.

(J) Loss of C1QBP increases chromosome abnormalities. Metaphase spread assays were performed using C1QBP-wild type and C1QBP-knockout HeLa cells; chromosome abnormalities were counted in over 200 cells each. The data are presented as means ± SD ($n = 3$, *$p < 0.05$, **$p < 0.01$).

See also Figure S6.

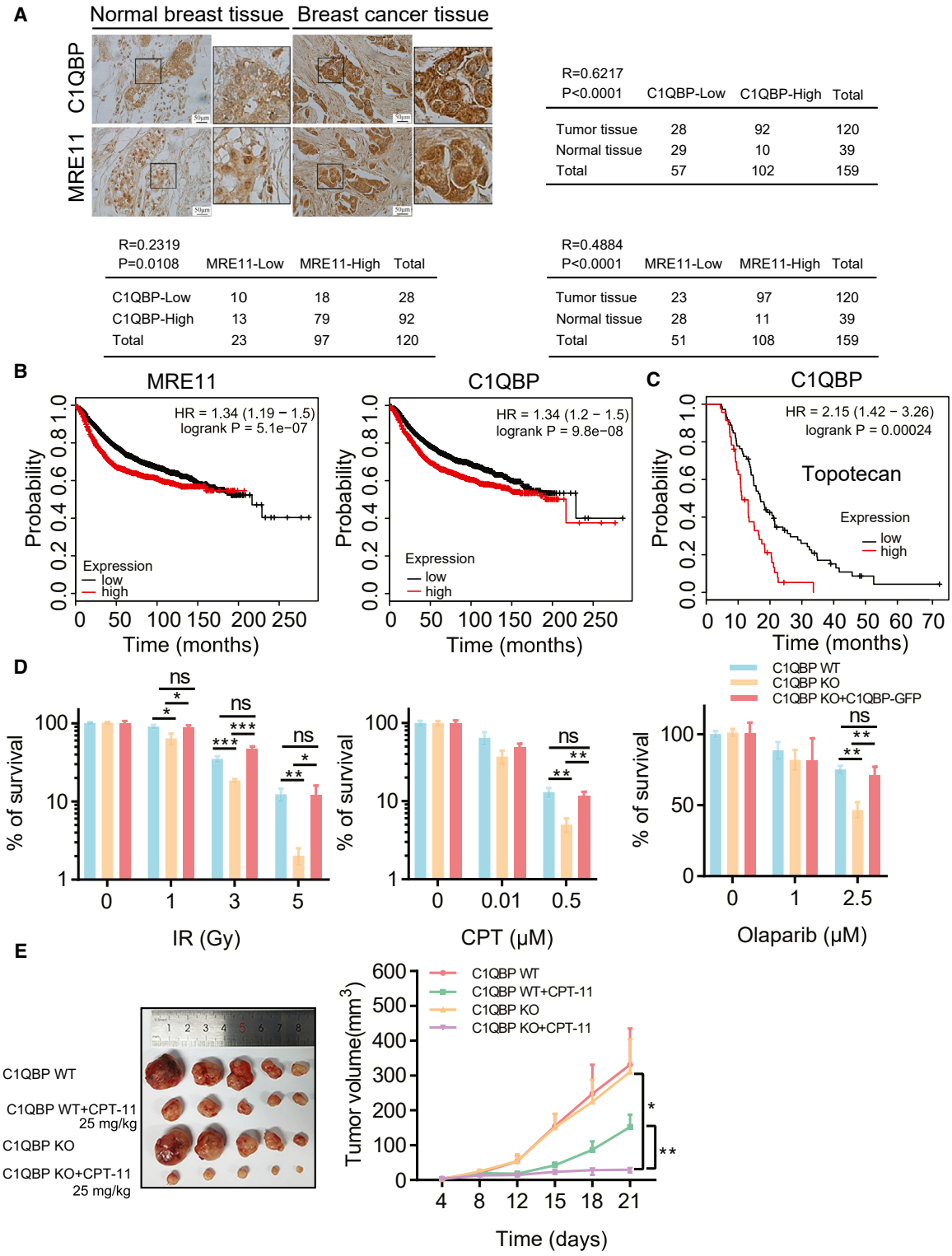

Figure 7. C1QBP Is a Potential Therapeutic Target for Cancer Treatment

(A) Immunohistochemical staining of C1QBP and MRE11 was performed using a breast tissue microarray. Correlation analyses between C1QBP and MRE11 in normal breast and breast carcinoma samples are shown in tables.

(B) Kaplan-Meier survival curve for the overall survival of breast cancer patients with low and high expression of C1QBP or MRE11. The hazard ratio (HR) and log-rank p value are indicated in each panel.

(legend continued on next page)

DNA damage repair pathways. In this study, we found that MRE11/RAD50 unexpectedly forms MRC complex with C1QBP to regulate the MRE11-mediated DDR pathway. C1QBP stabilizes and maintains the MRE11 protein pool but prevents MRE11 association with chromatin and limits its enzymatic activity under normal conditions. Upon DNA damage, ATM-mediated MRE11 phosphorylation dismisses the MRC complex and promotes the MRN complex assembly at DNA damage sites to initiate DNA end resection. After completing DNA end resection, C1QBP might help MRE11 dissociate from chromatin, followed by formation of the MRC complex again. Overall, C1QBP functions as a molecular sponge, maintaining the MRE11/RAD50 protein pool while limiting its enzyme activity.

MRE11 is the central nuclease component of the MRN complex binds damaged DNA and nucleolytically processes the resection of DNA ends, a function that is key to initiate HR and inhibit the NHEJ repair pathway (Paull, 2018). Although inefficient end resection would limit precise homologous recombination, uncontrolled MRE11 might degrade nascent DNA strands and impair genomic stability (Hashimoto et al., 2010; Ray Chaudhuri et al., 2016; Schlacher et al., 2011). Recently, it has been reported that DYNLL1 directly binds to MRE11 to limit DNA end resection in BRCA1-deficient cells and UBQLN4 removes ubiquitylated MRE11 from damaged chromatin (He et al., 2018; Jachimowicz et al., 2019). We also provide evidence that C1QBP binds directly to MRE11 to stabilize MRE11 and limit its DNA end resection activity.

C1QBP is an evolutionarily conserved acidic protein first identified as the complement component C1q-binding protein (Storrs et al., 1981). C1QBP is ubiquitously expressed in all somatic cells, with the exception of red blood cells (Ghebrehiwet and Peerschke, 2004). The precise role of C1QBP *in vivo* is poorly understood because of embryonic lethality in systemic C1QBP-deficient mice (Yagi et al., 2012). Moreover, C1QBP is highly upregulated in many types of tumors and correlates with resistance to chemotherapy (Ghebrehiwet and Peerschke, 2004; Peerschke and Ghebrehiwet, 2014; Shen et al., 2014). Interatomic analysis has revealed that C1QBP is associated with cancer cell chemotaxis and metastasis (Zhang et al., 2013). Our data also showed that a high level of C1QBP expression was associated with a worse overall survival and resistance to conventional chemotherapy. It was reported that C1QBP binds to ARF and is required for ARF-induced apoptosis (Itahana and Zhang, 2008). Although C1QBP predominantly localized in mitochondria as well as in the cytosol, it also has been reported that C1QBP distributed and played functions in nucleus (Ghebrehiwet and Peerschke, 2004). *Drosophila* C1QBP is a core histone chaperone that participated in chromatin remodeling in nucleus (Emelyanov et al., 2014), and C1QBP translocated to nucleus upon cisplatin treatment in HeLa cells (Kamal and Datta, 2006). We also observed that C1QBP shows significantly increased nuclear translocation after CPT long time treatment, suggesting that C1QBP might help MRE11 dissociate from DNA upon completion of DNA repair, followed by formation of the MRC complex again.

An interesting feature of C1QBP protein is its high negative-charge density and asymmetric charge distribution, suggesting its possible association with positively charged proteins (Jiang et al., 1999). Our study revealed that C1QBP directly interacts with MRE11 by recognizing its GAR motif and stabilizes MRE11 *in vivo* and *in vitro*. The molecular mechanism of this interaction may be due to binding facilitated by the acidic structure and high negative-charge density of C1QBP and positive charge of the MRE11 arginine-rich motif (Jiang et al., 1999). Nonetheless, we failed to identify which region of C1QBP is required to interact with MRE11 because deletion of any small region of C1QBP destabilizes it, suggesting that internal deletion may destroy the structure of C1QBP.

The level of MRE11 protein is crucial for efficient DNA repair, although uncontrolled MRE11 might mediate the degradation of nascent DNA strands (Hashimoto et al., 2010; Paull and Gellert, 1998; Ray Chaudhuri et al., 2016; Vallerga et al., 2015). To avoid nonspecific DNA association and cleavage by excess MRE11, C1QBP interacts with it to prevent its DNA binding. We believe that the high negative-charge density of C1QBP sequesters the MRC complex away from DNA, which is also negatively charged. We speculate that C1QBP could affect both exo- and endonuclease activity by preventing the DNA binding of MRE11/RAD50. It has been reported that MR exhibits a robust endonuclease activity on duplex DNA only by forming MRN-CtIP complex (Anand et al., 2016; Cannavo and Cejka, 2014). Our future work will keep trying to figure out the inhibitory effect of C1QBP on the endonucleolytic processing of DSB ends.

In vitro C1QBP can displace DNA from the MRE11/RAD50/DNA complex (Figure 2H), but DNA cannot disturb MRC complex formation, suggesting that C1QBP binds MRE11 with higher affinity and could help MRE11 dissociate with chromatin upon completion of DNA resection. We also showed that the loss of C1QBP *in vivo* promotes the nonspecific association of MRE11 with unbroken chromatin and retards MRE11 recruitment to DSBs upon DNA damage (Figure 5). Recruitment of MRE11 to the site of DNA damage is one of the earliest events of DDR and is required for activating DNA repair and cell-cycle checkpoint pathways. Therefore, expeditious and accurate MRE11 recruitment to damaged DNA should be tightly regulated because either delayed recruitment or nonspecific association with undamaged DNA would retard MRE11-mediated DNA end resection. We revealed that C1QBP prevents MRE11 nonspecific association with undamaged chromatin and facilitates MRE11 recruitment to DSBs upon DNA damage.

Our data also indicate that C1QBP association with MRE11 is required to maintain a certain amount of MRE11 in

(C) Kaplan-Meier plots showing the overall survival in ovarian cancer patients treated with Topotecan with low and high expression of C1QBP. The hazard ratio (HR) and log-rank p value are indicated in each panel.

(D) Control cells and C1QBP-knockout HeLa cells were treated with the control or indicated dose of CPT (2 h), IR, or olaparib (24 h), and cell survival rates were counted by calculating the colony numbers. The data are presented as means ± SD (n = 3, *p < 0.05, **p < 0.01, ***p < 0.001; ns, no significance).

(E) Deletion of C1QBP enhances tumor regression due to chemotherapy. C1QBP-wild type or C1QBP-knockout A375 cells were used in a xenograft tumor assay with camptothecin-11 (CPT-11) treatment, and tumor weights were quantified (n ≥ 5 mice, mean ± SEM, *p < 0.05, **p < 0.01).

anticipation of damaged DNA repair and to prevent MRE11 association with chromatin and limit its enzymatic activity under normal conditions. In response to DNA damage, ATM-mediated MRE11 S676/S678 phosphorylation dissociates the MRC complex and releases MRE11/RAD50 to assemble the MRN complex and initiate DNA end resection, indicating that the change in charge affects the conformation and the assembly of MRC complex. It was reported that the MRE11-S676A/S678A mutated cell line showed decreased cell survival and increased chromosomal aberrations after radiation exposure, indicating a defect in DNA repair (Kijas et al., 2015). We also found that the MRE11 R572Q/R576Q mutant with the loss of C1QBP-binding ability failed to restore the DNA repair capacity of MRE11-depleted cells. These data indicate that both the interaction and the dissociation of MRE11 and C1QBP are crucial for efficient DNA repair.

In this study, we identified an unexpected small protein, C1QBP, which modulates DDR by regulating MRE11 at multiple levels. C1QBP forms a complex (MRC) with MRE11/RAD50 to maintain the MRE11 protein pool but limit MRE11 activity under normal conditions. Upon DNA damage, ATM-mediated phosphorylation of MRE11 results in its dissociation from the MRC complex and promotes MRE11-mediated DNA end resection. C1QBP is highly expressed in breast cancer and positively correlates with MRE11 expression, and inhibition of C1QBP enhances tumor regression with chemotherapy. Taken together, our findings reveal that C1QBP is a novel important player in the DNA damage response and suggest that C1QBP may serve as a therapeutic target for cancer treatments.

STAR★METHODS

Detailed methods are provided in the online version of this paper and include the following:

SUPPLEMENTAL INFORMATION

Supplemental Information can be found online at https://doi.org/10.1016/j.molcel.2019.06.023.

ACKNOWLEDGMENTS

We thank Drs. Mo Li (Peking University Third Hospital), Huadong Pei (Beijing Institute of Lifeomics), and Xiaofeng Zheng (Peking University) for reagents and technical help. We thank all members of the Wang laboratory for insightful discussion and technical assistance. This study was supported by the National Key R&D Program of China (2016YFC1302100 and 2017YFA0503900), the National Natural Science Foundation of China (81672981, 81872282, 81621063, 81803017, and 81661128008), NIH (RO1ES007061), Beijing Municipal Natural Science Foundation (7182082), Peking University (BMU20140367), and the Young Talent 1000 Project (QNQR201602).

AUTHOR CONTRIBUTIONS

Conceptualization, Y.B., W.W., and J.W.; Investigation, Y.B., W.W., S.L., J.Z., H.L., M. Zhao, S.L., P.S., X.L., and J.W.; Writing, Y.B., W.W., and J.W.; Resources, Q.S. and M. Zhou; Drawing, Y.H.; Discussion, X.A.Z., H.Z., J.L., W.G.-Z., and X.X.; Supervision, W.W. and J.W.

DECLARATION OF INTERESTS

The authors declare no competing interests.

Received: February 14, 2019
Revised: May 6, 2019
Accepted: June 18, 2019
Published: July 25, 2019

REFERENCES

Anand, R., Ranjha, L., Cannavo, E., and Cejka, P. (2016). Phosphorylated CtIP Functions as a Co-factor of the MRE11-RAD50-NBS1 Endonuclease in DNA End Resection. Mol. Cell *64*, 940–950.

Assenmacher, N., and Hopfner, K.P. (2004). MRE11/RAD50/NBS1: complex activities. Chromosoma *113*, 157–166.

Berkovich, E., Monnat, R.J., Jr., and Kastan, M.B. (2007). Roles of ATM and NBS1 in chromatin structure modulation and DNA double-strand break repair. Nat. Cell Biol. *9*, 683–690.

Boisvert, F.M., Déry, U., Masson, J.Y., and Richard, S. (2005). Arginine methylation of MRE11 by PRMT1 is required for DNA damage checkpoint control. Genes Dev. *19*, 671–676.

Buis, J., Wu, Y., Deng, Y., Leddon, J., Westfield, G., Eckersdorff, M., Sekiguchi, J.M., Chang, S., and Ferguson, D.O. (2008). Mre11 nuclease activity has essential roles in DNA repair and genomic stability distinct from ATM activation. Cell *135*, 85–96.

Caminsky, N.G., Mucaki, E.J., Perri, A.M., Lu, R., Knoll, J.H., and Rogan, P.K. (2016). Prioritizing Variants in Complete Hereditary Breast and Ovarian Cancer Genes in Patients Lacking Known BRCA Mutations. Hum. Mutat. *37*, 640–652.

Cannavo, E., and Cejka, P. (2014). Sae2 promotes dsDNA endonuclease activity within Mre11-Rad50-Xrs2 to resect DNA breaks. Nature *514*, 122–125.

Carney, J.P., Maser, R.S., Olivares, H., Davis, E.M., Le Beau, M., Yates, J.R., 3rd, Hays, L., Morgan, W.F., and Petrini, J.H. (1998). The hMre11/hRad50 protein complex and Nijmegen breakage syndrome: linkage of double-strand break repair to the cellular DNA damage response. Cell *93*, 477–486.

Cejka, P. (2015). DNA End Resection: Nucleases Team Up with the Right Partners to Initiate Homologous Recombination. J. Biol. Chem. *290*, 22931–22938.

Chang, L., Huang, J., Wang, K., Li, J., Yan, R., Zhu, L., Ye, J., Wu, X., Zhuang, S., Li, D., and Zhang, G. (2016). Targeting Rad50 sensitizes human nasopharyngeal carcinoma cells to radiotherapy. BMC Cancer *16*, 190.

Cruz-García, A., López-Saavedra, A., and Huertas, P. (2014). BRCA1 accelerates CtIP-mediated DNA-end resection. Cell Rep. *9*, 451–459.

Deshpande, R.A., Williams, G.J., Limbo, O., Williams, R.S., Kuhnlein, J., Lee, J.H., Classen, S., Guenther, G., Russell, P., Tainer, J.A., and Paull, T.T. (2014). ATP-driven Rad50 conformations regulate DNA tethering, end resection, and ATM checkpoint signaling. EMBO J. *33*, 482–500.

Deshpande, R.A., Lee, J.H., Arora, S., and Paull, T.T. (2016). Nbs1 Converts the Human Mre11/Rad50 Nuclease Complex into an Endo/Exonuclease Machine Specific for Protein-DNA Adducts. Mol. Cell *64*, 593–606.

Deshpande, R.A., Lee, J.H., and Paull, T.T. (2017). Rad50 ATPase activity is regulated by DNA ends and requires coordination of both active sites. Nucleic Acids Res. *45*, 5255–5268.

Di Marco, S., Hasanova, Z., Kanagaraj, R., Chappidi, N., Altmannova, V., Menon, S., Sedlackova, H., Langhoff, J., Surendranath, K., Huhn, D., et al. (2017). RECQ5 Helicase Cooperates with MUS81 Endonuclease in Processing Stalled Replication Forks at Common Fragile Sites during Mitosis. Mol. Cell *66*, 658–671.

Dolganov, G.M., Maser, R.S., Novikov, A., Tosto, L., Chong, S., Bressan, D.A., and Petrini, J.H. (1996). Human Rad50 is physically associated with human Mre11: identification of a conserved multiprotein complex implicated in recombinational DNA repair. Mol. Cell. Biol. *16*, 4832–4841.

Duursma, A.M., Driscoll, R., Elias, J.E., and Cimprich, K.A. (2013). A role for the MRN complex in ATR activation via TOPBP1 recruitment. Mol. Cell *50*, 116–122.

Emelyanov, A.V., Rabbani, J., Mehta, M., Vershilova, E., Keogh, M.C., and Fyodorov, D.V. (2014). Drosophila TAP/p32 is a core histone chaperone that cooperates with NAP-1, NLP, and nucleophosmin in sperm chromatin remodeling during fertilization. Genes Dev. *28*, 2027–2040.

Ghebrehiwet, B., and Peerschke, E.I. (2004). cC1q-R (calreticulin) and gC1q-R/p33: ubiquitously expressed multi-ligand binding cellular proteins involved in inflammation and infection. Mol. Immunol. *41*, 173–183.

Haber, J.E. (1998). The many interfaces of Mre11. Cell *95*, 583–586.

Hashimoto, Y., Ray Chaudhuri, A., Lopes, M., and Costanzo, V. (2010). Rad51 protects nascent DNA from Mre11-dependent degradation and promotes continuous DNA synthesis. Nat. Struct. Mol. Biol. *17*, 1305–1311.

He, Y.J., Meghani, K., Caron, M.C., Yang, C., Ronato, D.A., Bian, J., Sharma, A., Moore, J., Niraj, J., Detappe, A., et al. (2018). DYNLL1 binds to MRE11 to limit DNA end resection in BRCA1-deficient cells. Nature *563*, 522–526.

Herdendorf, T.J., Albrecht, D.W., Benkovic, S.J., and Nelson, S.W. (2011). Biochemical characterization of bacteriophage T4 Mre11-Rad50 complex. J. Biol. Chem. *286*, 2382–2392.

Hoa, N.N., Shimizu, T., Zhou, Z.W., Wang, Z.Q., Deshpande, R.A., Paull, T.T., Akter, S., Tsuda, M., Furuta, R., Tsutsui, K., et al. (2016). Mre11 Is Essential for the Removal of Lethal Topoisomerase 2 Covalent Cleavage Complexes. Mol. Cell *64*, 580–592.

Itahana, K., and Zhang, Y. (2008). Mitochondrial p32 is a critical mediator of ARF-induced apoptosis. Cancer Cell *13*, 542–553.

Jachimowicz, R.D., Beleggia, F., Isensee, J., Velpula, B.B., Goergens, J., Bustos, M.A., Doll, M.A., Shenoy, A., Checa-Rodriguez, C., Wiederstein, J.L., et al. (2019). UBQLN4 Represses Homologous Recombination and Is Overexpressed in Aggressive Tumors. Cell *176*, 505–519.e22.

Jiang, J., Zhang, Y., Krainer, A.R., and Xu, R.M. (1999). Crystal structure of human p32, a doughnut-shaped acidic mitochondrial matrix protein. Proc. Natl. Acad. Sci. USA *96*, 3572–3577.

Kamal, A., and Datta, K. (2006). Upregulation of hyaluronan binding protein 1 (HABP1/p32/gC1qR) is associated with Cisplatin induced apoptosis. Apoptosis *11*, 861–874.

Kijas, A.W., Lim, Y.C., Bolderson, E., Cerosaletti, K., Gatei, M., Jakob, B., Tobias, F., Taucher-Scholz, G., Gueven, N., Oakley, G., et al. (2015). ATM-dependent phosphorylation of MRE11 controls extent of resection during homology directed repair by signalling through Exonuclease 1. Nucleic Acids Res. *43*, 8352–8367.

Lammens, K., Bemeleit, D.J., Möckel, C., Clausing, E., Schele, A., Hartung, S., Schiller, C.B., Lucas, M., Angermüller, C., Söding, J., et al. (2011). The Mre11:Rad50 structure shows an ATP-dependent molecular clamp in DNA double-strand break repair. Cell *145*, 54–66.

Lee, J.H., and Paull, T.T. (2005). ATM activation by DNA double-strand breaks through the Mre11-Rad50-Nbs1 complex. Science *308*, 551–554.

Levikova, M., Pinto, C., and Cejka, P. (2017). The motor activity of DNA2 functions as an ssDNA translocase to promote DNA end resection. Genes Dev. *31*, 493–502.

Matsuoka, S., Ballif, B.A., Smogorzewska, A., McDonald, E.R., 3rd, Hurov, K.E., Luo, J., Bakalarski, C.E., Zhao, Z., Solimini, N., Lerenthal, Y., et al. (2007). ATM and ATR substrate analysis reveals extensive protein networks responsive to DNA damage. Science *316*, 1160–1166.

Matsuura, S., Tauchi, H., Nakamura, A., Kondo, N., Sakamoto, S., Endo, S., Smeets, D., Solder, B., Belohradsky, B.H., Der Kaloustian, V.M., et al. (1998). Positional cloning of the gene for Nijmegen breakage syndrome. Nat. Genet. *19*, 179–181.

Mimitou, E.P., and Symington, L.S. (2008). Sae2, Exo1 and Sgs1 collaborate in DNA double-strand break processing. Nature *455*, 770–774.

Paull, T.T. (2018). 20 Years of Mre11 Biology: No End in Sight. Mol. Cell *71*, 419–427.

Paull, T.T., and Deshpande, R.A. (2014). The Mre11/Rad50/Nbs1 complex: recent insights into catalytic activities and ATP-driven conformational changes. Exp. Cell Res. *329*, 139–147.

Paull, T.T., and Gellert, M. (1998). The 3′ to 5′ exonuclease activity of Mre 11 facilitates repair of DNA double-strand breaks. Mol. Cell *1*, 969–979.

Paull, T.T., and Gellert, M. (1999). Nbs1 potentiates ATP-driven DNA unwinding and endonuclease cleavage by the Mre11/Rad50 complex. Genes Dev. *13*, 1276–1288.

Peerschke, E.I., and Ghebrehiwet, B. (2014). cC1qR/CR and gC1qR/p33: observations in cancer. Mol. Immunol. *61*, 100–109.

Ray Chaudhuri, A., Callen, E., Ding, X., Gogola, E., Duarte, A.A., Lee, J.E., Wong, N., Lafarga, V., Calvo, J.A., Panzarino, N.J., et al. (2016). Replication fork stability confers chemoresistance in BRCA-deficient cells. Nature *535*, 382–387.

Reginato, G., Cannavo, E., and Cejka, P. (2017). Physiological protein blocks direct the Mre11-Rad50-Xrs2 and Sae2 nuclease complex to initiate DNA end resection. Genes Dev. *31*, 2325–2330.

Rojas, E., Lopez, M.C., and Valverde, M. (1999). Single cell gel electrophoresis assay: methodology and applications. J. Chromatogr. B Biomed. Sci. Appl. *722*, 225–254.

Schiller, C.B., Lammens, K., Guerini, I., Coordes, B., Feldmann, H., Schlauderer, F., Möckel, C., Schele, A., Strässer, K., Jackson, S.P., and Hopfner, K.P. (2012). Structure of Mre11-Nbs1 complex yields insights into ataxia-telangiectasia-like disease mutations and DNA damage signaling. Nat. Struct. Mol. Biol. *19*, 693–700.

Schlacher, K., Christ, N., Siaud, N., Egashira, A., Wu, H., and Jasin, M. (2011). Double-strand break repair-independent role for BRCA2 in blocking stalled replication fork degradation by MRE11. Cell *145*, 529–542.

Shen, X., Han, B., Shen, Y., Yang, J., Ren, T., Sha, G., and Xiang, Y. (2014). [Expression of C1QBP gene and its correlation with drug resistance in human resistance choriocarcinoma cell line]. Zhonghua Fu Chan Ke Za Zhi *49*, 616–620.

Song, J., Wang, T., Xu, W., Wang, P., Wan, J., Wang, Y., Zhan, J., and Zhang, H. (2018). HOXB9 acetylation at K27 is responsible for its suppression of colon cancer progression. Cancer Lett. *426*, 63–72.

Stewart, G.S., Maser, R.S., Stankovic, T., Bressan, D.A., Kaplan, M.I., Jaspers, N.G.J., Raams, A., Byrd, P.J., Petrini, J.H.J., and Taylor, A.M.R. (1999). The

DNA double-strand break repair gene hMRE11 is mutated in individuals with an ataxia-telangiectasia-like disorder. Cell *99*, 577–587.

Storrs, S.B., Kolb, W.P., Pinckard, R.N., and Olson, M.S. (1981). Characterization of the binding of purified human C1q to heart mitochondrial membranes. J. Biol. Chem. *256*, 10924–10929.

Taylor, A.M.R., Groom, A., and Byrd, P.J. (2004). Ataxia-telangiectasia-like disorder (ATLD)-its clinical presentation and molecular basis. DNA Repair (Amst.) *3*, 1219–1225.

Trujillo, K.M., Yuan, S.S., Lee, E.Y., and Sung, P. (1998). Nuclease activities in a complex of human recombination and DNA repair factors Rad50, Mre11, and p95. J. Biol. Chem. *273*, 21447–21450.

Vallerga, M.B., Mansilla, S.F., Federico, M.B., Bertolin, A.P., and Gottifredi, V. (2015). Rad51 recombinase prevents Mre11 nuclease-dependent degradation and excessive PrimPol-mediated elongation of nascent DNA after UV irradiation. Proc. Natl. Acad. Sci. USA *112*, E6624–E6633.

Wang, W., Daley, J.M., Kwon, Y., Krasner, D.S., and Sung, P. (2017). Plasticity of the Mre11-Rad50-Xrs2-Sae2 nuclease ensemble in the processing of DNA-bound obstacles. Genes Dev. *31*, 2331–2336.

Williams, G.J., Lees-Miller, S.P., and Tainer, J.A. (2010). Mre11-Rad50-Nbs1 conformations and the control of sensing, signaling, and effector responses at DNA double-strand breaks. DNA Repair (Amst.) *9*, 1299–1306.

Wu, J., Zhang, X., Zhang, L., Wu, C.Y., Rezaeian, A.H., Chan, C.H., Li, J.M., Wang, J., Gao, Y., Han, F., et al. (2012). Skp2 E3 ligase integrates ATM activation and homologous recombination repair by ubiquitinating NBS1. Mol. Cell *46*, 351–361.

Xie, B., Zhang, L., Zhao, H., Bai, Q., Fan, Y., Zhu, X., Yu, Y., Li, R., Liang, X., Sun, Q.Y., et al. (2018). Poly(ADP-ribose) mediates asymmetric division of mouse oocyte. Cell Res. *28*, 462–475.

Xu, L., Xiao, N., Liu, F., Ren, H., and Gu, J. (2009). Inhibition of RIG-I and MDA5-dependent antiviral response by gC1qR at mitochondria. Proc. Natl. Acad. Sci. USA *106*, 1530–1535.

Yadav, S., Reeves, A., Campian, S., Paine, A., and Zakalik, D. (2017). Outcomes of retesting BRCA negative patients using multigene panels. Fam. Cancer *16*, 319–328.

Yagi, M., Uchiumi, T., Takazaki, S., Okuno, B., Nomura, M., Yoshida, S., Kanki, T., and Kang, D. (2012). p32/gC1qR is indispensable for fetal development and mitochondrial translation: importance of its RNA-binding ability. Nucleic Acids Res. *40*, 9717–9737.

Yamaguchi-Iwai, Y., Sonoda, E., Buerstedde, J.M., Bezzubova, O., Morrison, C., Takata, M., Shinohara, A., and Takeda, S. (1998). Homologous recombination, but not DNA repair, is reduced in vertebrate cells deficient in RAD52. Mol. Cell. Biol. *18*, 6430–6435.

Yu, Z., Vogel, G., Coulombe, Y., Dubeau, D., Spehalski, E., Hébert, J., Ferguson, D.O., Masson, J.Y., and Richard, S. (2012). The MRE11 GAR motif regulates DNA double-strand break processing and ATR activation. Cell Res. *22*, 305–320.

Zhang, X., Zhang, F., Guo, L., Wang, Y., Zhang, P., Wang, R., Zhang, N., and Chen, R. (2013). Interactome analysis reveals that C1QBP (complement component 1, q subcomponent binding protein) is associated with cancer cell chemotaxis and metastasis. Mol. Cell. Proteomics *12*, 3199–3209.

Zhong, Z.H., Jiang, W.Q., Cesare, A.J., Neumann, A.A., Wadhwa, R., and Reddel, R.R. (2007). Disruption of telomere maintenance by depletion of the MRE11/RAD50/NBS1 complex in cells that use alternative lengthening of telomeres. J. Biol. Chem. *282*, 29314–29322.

Zhou, H., Kawamura, K., Yanagihara, H., Kobayashi, J., and Zhang-Akiyama, Q.M. (2017). NBS1 is regulated by two kind of mechanisms: ATM-dependent complex formation with MRE11 and RAD50, and cell cycle-dependent degradation of protein. J. Radiat. Res. (Tokyo) *58*, 487–494.

STAR★METHODS

KEY RESOURCES TABLE

REAGENT or RESOURCE	SOURCE	IDENTIFIER
Antibodies		
Mouse anti-C1QBP(Immunofluorescence)	Abcam	Cat#: ab24733; RRID: AB_448269
Rabbit anti-C1QBP(Immunoblot)	ABclonal	Cat#: A1883; RRID: AB_2763916
Rabbit anti-MRE11(Immunoblot)	Novus	Cat#: NB100-142; RRID: AB_10077796
Rabbit anti-MRE11(Immunofluorescence)	Abcam	Cat#: ab33125; RRID: AB_776530
Rabbit anti-RAD50	ABclonal	Cat#: A3078; RRID: AB_2764881
Rabbit anti-NBS1	Proteintech	Cat#: 55025-1-AP; RRID: AB_10858928
Mouse anti-Flag	Sigma-Aldrich	Cat#: F3165; RRID: AB_259529
Mouse anti-Flag	Sigma-Aldrich	Cat#: A8592; RRID: AB_439702
Mouse anti-c-Myc	Santa Cruz	Cat#: sc-40(9E10); RRID: AB_627268
Mouse anti-GFP	Sungene Biotech	Cat#: KM8009
Rabbit anti-dimethyl-Arginine,asymmetric (ASYM25)	Millipore	Cat#:09-814; RRID: AB_10615495
Rabbit anti-RPA32	Proteintech	Cat#:10412-1-AP; RRID: AB_2269665
Mouse anti-Chk1	Santa Cruz	Cat#: sc-8408; RRID: AB_627257
Rabbit anti-phospho-RPA32(S4/S8)	Abcam	Cat#: ab87277; RRID: AB_1952482
Rabbit anti-phospho-RPA32(T21)	HUABIO	Cat#: ET1611-18
Rabbit anti-phospho-Chk1(S345)	CST	Cat#: 2348S; RRID: AB_331212
Rabbit anti-phospho- Chk1(S317)	CST	Cat#:12302S
Rabbit anti-phospho- NBS1(S343)	CST	Cat#: 3001S; RRID: AB_10829154
Rabbit anti-phospho-ATM(S1981)	CST	Cat#: 5883S; RRID: AB_10835213
Rabbit anti-RAD51(Immunoblot)	Abcam	Cat#: ab133534; RRID: AB_2722613
Mouse anti-RAD51(Immunofluorescence)	Novus	Cat#: NB100-148; RRID: AB_1002131
Mouse anti-CyclinA	Santa Cruz	Cat#: sc-271682; RRID: AB_10709300
Rabbit anti-CyclinA2	Abcam	Cat#: ab181591
Mouse anti-phospho-Histone H2A.X (Ser139)	Abcam	Cat#: ab26350; RRID: AB_470861
Mouse anti-phospho-Histone H2A.X clone JBW301	Millipore	Cat#: 05-636-I; RRID: AB_2755003
Rabbit anti-IgG	Biodragon	Cat#: BF01001
Mouse anti-His	Sigma-Aldrich	Cat#: A7058; RRID: AB_258326
Rabbit anti-CtIP	Bethyl	Cat#: A300-488A; RRID: AB_2175262
Mouse anti-MBP	NEB	Cat#: E8038; RRID: AB_1559738
Rabbit anti-BrdU	Abcam	Cat#: ab152095
Mouse anti-Histone H3	Biodragon	Cat#: B1055
Mouse anti-GAPDH	Sungene	Cat#: KM9002; RRID: AB_2721026
Mouse anti-α-Tubulin	Sungene	Cat#: KM9007L
Bacterial and Virus Strains		
DH5α	GenStar	Cat#: S101-02
BL21(DE3)	GenStar	Cat#: S106-02
Rosetta (DE3) pLysS	Novagen	Cat#: 71401
DH10Bac	GIBCO	Cat#: 10361012
Chemicals, Peptides, and Recombinant Proteins		
ATR Inhibitor VE-821	TargetMol	Cat#: T3032
ATM Inhibitor KU-55933	Selleck Chemicals	Cat#: S1092
Camptothecin(CPT)	HARVEYBIO	Cat#: HZB0043
Etoposide	HARVEYBIO	Cat#: HZB0098-25

(*Continued on next page*)

Continued

REAGENT or RESOURCE	SOURCE	IDENTIFIER
Adox	APExBIO	Cat#: APEB6120
BrdU	HARVEYBIO	Cat#: HZB1589-100
Cycloheximide	HARVEYBIO	Cat#: HZB0899-100
Micrococcal Nuclease	NEB	Cat#: M0247S
Olaparib	MedChem Express	Cat#: HY-10162
MG132	LABLEAD	Cat#: 474790LB
CPT-11	Meilunbio	Cat#: MB1126
Hydroxyurea	HARVEY	Cat#: HZB1502
Thymidine	HARVEYBIO	Cat#: HZB1595-1
Nocodazole	TargetMol	Cat#: T2802
Isopropyl β-D-thiogalactopyranoside (IPTG)	Merck	Cat#: CB420322
Trypsin	M&C	Cat#: CC017
GenOpti(IPTG-MEM)	M&C	Cat#: CT007
GAR/GAR(R576Q) peptides	DGpeptides Co.,Ltd	N/A
Critical Commercial Assays		
Cytoplasmic and nuclear separation kit	BestBio	Cat#: BB-36021
Deposited Data		
Original data	This study	https://doi.org/10.17632/495fbz3p92.1
Experimental Models: Cell Lines		
HEK293T	ATCC	CRL-11268c
HeLa	ATCC	CCL-2
Sf9	GIBCO	Cat#: 11496015
High Five	GIBCO	Cat#: B85502
Oligonucleotides		
siRNA targeting sequence: C1QBP: UCACGGUC ACUUUCAACAT	Itahana and Zhang, 2008	N/A
Recombinant DNA		
pEGFP-N1-C1QBP	This study	Available upon request
PDEST-N-SFB-MRE11/D1/D2/D3/D4/D5/D6/ DGAR/R570Q/R572Q/R576Q/R572/576Q/ S676/S678A mutants	This study	Available upon request
PDEST-C-SFB-C1QBP/C1QBP(S150A) mutants	This study	Available upon request
GST-C1QBP(74-282aa)	This study	Available upon request
pESC-MR-6xHis	This study	Available upon request
pET-C1QBP-flag	This study	Available upon request
pFastBac-NBS1	This study	Available upon request
Software and Algorithms		
Adobe Illustrator CC 2018	Adobe	https://www.adobe.com/
Adobe Photoshop CC 2018	Adobe	https://www.adobe.com/
ImageJ	NIH	https://imagej.nih.gov/ij/
Prism 7.0	Graphpad	https://www.graphpad.com/scientific-software/prism/
NIS ELEMENTS	Nikon	https://www.microscope.healthcare.nikon.com/
Other		
LR CLONASE II ENZYME MIX	invitrogen	Cat#: 11791020
BP CLONASE II ENZYME MIX	invitrogen	Cat#: 11789020
S-protein Agarose	Merck-Millipore	Cat#: 69704-4
STREPTAVIDIN SEPHAROSE HP	GE	Cat#: 17-5113-01

(*Continued on next page*)

Continued

REAGENT or RESOURCE	SOURCE	IDENTIFIER
Ni-NTA agarose	QIAGEN	Cat#: 30250
anti-Flag M2 affinity gel	Sigma	Cat#: A2220
Source 15Q	GE Healthcare	Cat#: 17094701
Source 15S	GE Healthcare	Cat#: 17094401
Q Sepharose	GE Healthcare	Cat#: 17051001
SP Sepharose	GE Healthcare	Cat#: 17072901

LEAD CONTACT AND MATERIALS AVAILABILITY

Further information and requests for resources and reagents should be directed to, and will be fulfilled by, the Lead Contact, Dr. Jiadong Wang (wangjd@bjmu.edu.cn).

EXPERIMENTAL MODEL AND SUBJECT DETAILS

HEK293T, HeLa and A375 cells were cultured in DMEM supplemented with 10% fetal bovine serum and 1% penicillin/streptomycin. All cells were incubated in a humidified ECSO incubator with 5% CO_2.

Animal experiments in this study were performed in accordance with the Guidelines of Peking University Animal Care and Use Committee. BALB/c female mice (5 weeks) were obtained from the Department of Laboratory Animal Science of Peking University Health Science Center (Beijing, China).

Source of bacterial and insect strains in this study is reported in the Key Resources Table.

METHOD DETAILS

Construction of Plasmids

cDNAs of MRE11, C1QBP, NBS1 and RAD50 were subcloned into pDONR201 (Invitrogen) as entry clones and subsequently transferred to gateway-compatible destination vectors for expression of N-tagged or C-tagged fusion proteins. All deletion and point mutants were generated by PCR and verified by sequencing.

Immunoprecipitation and Western Blotting

NETN buffer (20 mM Tris-HCl [pH 8.0], 100 mM NaCl, 1 mM EDTA, and 0.5% Nonidet P-40) was used to lyse cells with rotation at 4°C for 20 minutes. After the removal of cell debris by centrifugation (14,000 rpm for 10 minutes at 4°C), the soluble fractions were collected and incubated with S protein agarose (Merck-Millipore) for 4 hours at 4°C. The S protein beads were washed three times with NETN buffer and boiled with 2 × SDS loading buffer at 100°C for 8 minutes. The samples were then subjected to SDS-PAGE and immunoblotting with specific antibodies.

Soluble Fractions and Chromatin Fractions Extraction

The soluble fractions were acquired by using NETN buffer, after the centrifugation (14,000 rpm for 10 minutes at 4°C), the remaining were washed with PBS at least 3 times and lysed in cold EBC2 buffer (50 mM Tris-HCl [pH 7.5], 300 mM NaCl, 5 mM $CaCl_2$, and 10 U microcal nuclease). After sonication for about 20 s and centrifugation at 14,000 rpm for 15 minutes at 4°C, the supernatants were transferred to a fresh tube as chromatin fractions.

Tandem Affinity Purification (TAP)

293T cells stably expressing SFB-MRE11, NBS1-SFB, SFB-RAD50, C1QBP-SFB or SFB-MRE11-ΔGAR were lysed with NETN buffer on ice for 20 minutes. Cell lysates were centrifuged at 20,000 × g for 15 minutes, and the supernatants were incubated with streptavidin Sepharose beads for 2 hours at 4°C. The resin was washed three times with NETN buffer and eluted twice with elution buffer (2 mg/ml biotin, 20 mM Tris-HCl [pH 8.0], 100 mM NaCl, 1 mM EDTA, and 0.5% Nonidet P-40) for 6 hours at 4°C. The eluates were combined and then incubated with S-protein agarose (Novagen) for 4 hours at 4°C. The S beads were washed three times with NETN buffer. The proteins bound to the S-protein agarose beads were eluted with 40 μL of 1 × SDS loading buffer, separated by SDS-PAGE and then visualized by Coomassie Blue staining. The eluted proteins were identified by mass spectrometry analysis.

Expression and Purification of the MRE11/RAD50 Complex

The coding sequences for MRE11 and RAD50 with a C-terminal 6xHis tag were amplified by PCR and inserted into the pESC-URA vector, which generated pESC-MR-6xHis. The MR complex was overexpressed by introducing pESC-MR-6xHis into the

protease-deficient yeast strain YRP654 (MATα ura3-52 trp1Δ leu2Δ1 his3Δ200 pep4::HIS3 prb1Δ1.6R GAL). An overnight yeast culture was diluted 1:4 into 8 L of omission medium containing 2% galactose, 3% glycerol, and 3% lactic acid. After 24 hours of culture at 30°C, the cells were harvested and stored at −80°C. After being agitated with dry ice in a coffee grinder, the cell pellet (~30 g) was resuspended in 100 mL of T buffer (25 mM Tris-HCl, pH 7.5, 10% glycerol, 0.5 mM EDTA, 1 mM DTT, 0.01% Igepal) with 300 mM KCl and protease inhibitors (aprotinin, chymostatin, leupeptin and pepstatin A at 5 μg/ml each, 1 mM phenylmethylsulfonyl fluoride). The cell lysate was clarified by ultracentrifugation at 40,000 rpm for 1 hour, and the supernatant was constantly mixed with 4 mL of Ni-NTA agarose (QIAGEN) in the presence of 20 mM imidazole. After 1 h incubation, the resin was washed with 250 mL of T buffer containing 300 mM KCl and 20 mM imidazole. Bound MRE11/RAD50 protein was eluted with 6 mL of the same buffer containing 200 mM imidazole. The protein pool was diluted with T buffer and fractionated on a 2 mL Q Sepharose column (GE Healthcare) with a 40 mL gradient of 100-600 mM KCl in T buffer. The MRE11/RAD50 peak fractions were pooled, diluted with T buffer and further fractionated on a 1 mL Source 15S column (GE Healthcare) using the same buffer as above. Fractions containing purified MRE11/RAD50 were pooled, concentrated with a centrifugal filter (Millipore), and stored at −80°C in small aliquots. The yield of MRE11/RAD50 was ~200 μg from 8 L of cell culture. Flag tag was introduced into the C-terminal of MRE11 to improve MR complex purity. The procedure we used to purify Flag- and 6xHis-tagged MR complex was similar to that described above, with the modification that proteins eluted from Ni-NTA agarose were subsequently subjected to anti-Flag affinity purification.

Expression and Purification of C1QBP

The coding sequence for C1QBP with a C-terminal Flag tag was introduced into the pET-28b vector to generate pET-C1QBP-Flag. C1QBP was overexpressed by introducing pET-C1QBP-Flag into *E. coli* strain Rosetta (DE3) pLysS. When the cell culture reached an OD600 of 0.6-0.8, 0.1 mM IPTG was added to induce protein expression. After 14 h incubation at 16°C, cells were harvested and stored at −80°C. The cell pellet (~20 g from 3 L of cell culture) was resuspended in 50 mL of T buffer with 300 mM KCl and protease inhibitors as above. The clarified cell lysate was prepared by sonication followed by ultracentrifugation as above. The supernatant was incubated with 2 mL of anti-Flag M2 affinity gel (Sigma) with constant mixing for 2 h. After washing the resin with 250 mL of T buffer containing 300 mM KCl, bound proteins were eluted into 3 mL of T buffer containing 300 mM KCl and 250 ng/μl Flag peptide. The eluate was diluted with T buffer and further fractionated on a 1 mL Source 15Q column (GE Healthcare) with a 50 mL gradient of 100-600 mM KCl in T buffer. The fractions containing purified C1QBP were pooled, concentrated and stored at −80°C in small aliquots. The yield of C1QBP was ~500 μg from 3 L of cell culture.

Expression and Purification of NBS1

The coding sequence for NBS1 with an N-terminal Flag tag was amplified by PCR and inserted into pFastBac vector to generate pFastBac-NBS1. Bacmid and baculovirus were prepared in *E. coli* DH10Bac and *Spodoptera frugiperda* Sf9 cells, respectively, by following the manufacturer's protocol (Bac-to-Bac baculovirus expression system, Invitrogen). For NBS1 expression, *Trichoplusia ni* High Five cells were infected with high-titer P3 baculovirus. Cells were harvested after 46 h and stored at −80°C. The cell pellet (~5 g from 800 mL of culture) was suspended in 50 mL of T buffer with 300 mM KCl and protease inhibitors. The clarified cell lysate was prepared by sonication followed by ultracentrifugation as above. The supernatant was incubated with 2 mL of anti-Flag M2 affinity gel (Sigma) with constant mixing for 2 h. After washing the resin with 150 mL of T buffer containing 500 mM KCl, bound proteins were eluted into 3 mL of T buffer containing 300 mM KCl and 250 ng/μl Flag peptide. The eluate was diluted with T buffer and further fractionated in a 2 mL SP Sepharose column (GE Healthcare) with a 50 mL gradient of 100-400 mM KCl in T buffer. The fractions containing purified NBS1 were pooled, concentrated and stored at −80°C in small aliquots. The yield of NBS1 was ~80 μg from 800 mL of cell culture.

Affinity *in Vitro* Pull-down Assay

To examine interaction between C1QBP and MRE11/RAD50, 140 ng Flag-tagged C1QBP was mixed with 470 ng MRE11/RAD50 in 30 μL of T buffer containing 100 mM KCl (final concentration) and incubated on ice for 1 h; 15 μL of anti-Flag M2 affinity gel (Sigma) was added to capture the protein complex. After constant shaking during 2 h, the supernatant was removed, and the resin was washed three times with 200 μL of the same buffer. Bound proteins were eluted from the resin in 40 μL of 1 × SDS loading buffer (30 mM Tris-HCl, pH 6.8, 10% glycerol, 1% SDS and 0.01% bromophenol blue). The supernatant and eluate fractions were analyzed by western blotting with the indicated antibodies. To confirm interaction between NBS1 and MRE11/RAD50, Flag pull-down was performed as above except that 510 ng Flag-tagged NBS1 was used. To examine the interaction between C1QBP and MRE11, GST and GST-C1QBP (74-282 aa) purified from *E. coli* and bound on Glutathione Sepharose beads were incubated in NETN buffer 4 h with cell lysate that stably expressed SFB-MRE11. After incubation, the GST beads were washed four times with 400 mM NETN buffer and boiled in 2 × SDS loading buffer, and the proteins were analyzed by western blotting using the indicated antibodies.

Nuclease Reactions

To evaluate the effect of C1QBP on MRE11/RAD50 exonuclease activity, reactions were set up by premixing the indicated concentrations of MRE11/RAD50 and C1QBP in 12 μL of reaction buffer (25 mM Tris-HCl, pH 7.5, 2 mM $MnCl_2$, 1 mM DTT, 100 μg/ml BSA) containing 100 mM KCl (final concentration), followed by the addition of 4 nM dsDNA or overhang DNA substrate. After a 30 minutes incubation at 37°C, the nuclease reaction mixtures were analyzed according to a procedure described elsewhere (Wang et al., 2017).

Colony Formation Assay

HeLa control cells or C1QBP knockout cells were treated with the indicated dose of IR, CPT (2 hours) and Olaparib (24 hours). The same number of cells exposed to the different processes were plated in 60 mm dishes. After 14 days, the cells were washed with phosphate-buffered saline (PBS) and stained with 0.1% Coomassie brilliant blue in 10% ethanol for 30 minutes at room temperature. The stained dishes were washed with water, and the colonies were counted.

DNA Fibers Assay

DNA fiber analysis of DNA end resection was performed as described previously with slight modifications (Cruz-García et al., 2014). Briefly, cells either expressing or depleted of C1QBP were grown in the presence of 10 μM BrdU (GE Healthcare) for 24 hours. After treated with 10 μM CPT for 2 hours, cells were harvested and resuspended in lysis buffer (200 mM Tris-HCl, pH 7.5, 50 mM EDTA and 0.5% SDS) to extract DNA. Cell lysates were then dripped onto a glass slide and DNA fibers were stretched along the slide after 5 minutes incubation. Glass slides were air-dried and fixed in 3:1 methanol/acetic acid solution at 4°C for 1 hour, followed by blocking in PBST buffer contacting 3% BSA for 20 minutes. DNA fibers without denaturation were incubated with an anti-BrdU antibody (Abcam) at 37°C for 1 hour. After washing with PBST three times, the slides were incubated with an Alexa Fluor 488-conjugated secondary antibody (ZSGB-Bio) for 45 minutes. Finally, the slides were mounted in a pre-cooled mounting reagent (Solarbio), and DNA fibers were observed with Nikon NI-E microscope. For each sample, at least 100 DNA fibers were analyzed.

Preparation and Analysis of Chromosome Spreads

The chromosome spreads assay was described previously (Di Marco et al., 2017). Briefly, the wild-type HeLa cells and C1QBP knockout HeLa cells were treated with nocodazole (200 ng/ml) for 5 hours. Cells were collected by mitotic shake-off and centrifuged for 5 minutes at 4°C (2000 g), and the pellet resuspended in 1 mL of DMEM. The suspensions were added 6 mL of 75 mM KCl (prewarmed to 37°C) and incubated for 15 minutes at 37°C. Each incubation was added 5 mL of Carnoy's buffer (75% methanol, 25% glacial acetic acid). And cells were then spread on slides and let slides air dry in dark. The dried slides were stained with Giemsa for 30 minutes. Chromosome spreads were counted in over 200 cells each. The data are presented as means ± SD (n = 3, *$p < 0.05$, **$p < 0.01$).

Single-Cell Gel Electrophoresis (SCGE)/Comet Assay

The SCGE comet assay was described previously (Rojas et al., 1999). Briefly, the media was removed, and then 0.005% Trypsin was added to the cells. Next, the cells were suspended in 500 μL of PBS for later use. Thereafter, 100 μL of 0.6% normal melting agarose (NMA) was added to the frosted glass slides. Coverslips (22 mm × 22 mm) were then quickly applied to the slides, which were placed flat at 4°C for 10 minutes. The coverslips were removed carefully, the cell suspensions were mixed with an equal volume of 1% low-melting agarose, followed by quickly adding 100 μL of the mixtures to the solidified NMA, covering the coverslips, placing them flat at 4°C for 10 minutes, and carefully removing them. The slides were placed overnight in cell lysis buffer prepared fresh at 4°C. Next, the glass slides were rinsed with ddH_2O and then were placed in precooled alkaline electrophoresis buffer for 20 minutes, followed by electrophoresis at 4°C for 30 minutes at 20 V and 200 mA. The slides were then neutralized twice with neutralization buffer for 15 minutes each time. Thereafter, the glass slides were removed and stained with 5 μg/ml of propidium iodide for 10 minutes in the dark. The slides were washed with ddH_2O, and comet formation was observed under a fluorescence microscope (Zeiss AxioCam 503 color). The pictures were analyzed using CASP software (http://casplab.com/).

Electrophoretic Mobility Shift Assay

The indicated concentrations of MRE11/RAD50 in combination with or without C1QBP were mixed with dsDNA or overhang DNA substrate in 12 μL of reaction buffer (25 mM Tris-HCl, pH 7.5, 5 mM $MgCl_2$, 1 mM DTT, 100 μg/ml BSA, 2 mM ATP) containing 100 mM KCl (final concentration). After a 15 minutes incubation at 37°C, the reactions were mixed with 4 μL of 4 × loading buffer (20 mM Tris-HCl, pH 7.5, 40% glycerol, 2 mM EDTA, 0.2% orange G) before electrophoresis through a 0.3% agarose gel in SB buffer (10 mM NaOH, 40 mM boric acid, pH 8.0). The gels were dried onto positively charged nylon membranes (GE Healthcare) and subjected to phosphorimaging analysis.

Generation of CRISPR-Cas9 knockout cell lines

The C1QBP knockout was generated in HeLa and A375 cells using the following gRNA: C1QBP gRNA-1 (exon-1): GTGCTGGGCTCCTCCGTCGCCGG; C1QBP gRNA-2 (exon-6): AGTGTTGTCCACCCCTCGGTCGG. MRE11-reconstituted HeLa cells were generated by cotransfection with SFB-MRE11 or SFB-MRE11-R572Q/R576Q and MRE11 gRNA: CAATCATGACGATCC CACAGGGG, which target the MRE11 sequence at the intron-exon-5 boundary. All C1QBP-knockout cells were confirmed by genomic sequence and immunoblotting.

Biotin-peptide Pull-Down Assay

A total of 2 μg or 8 μg of biotin-GAR or biotin-GAR (R576Q) and 30 μL of streptavidin Sepharose beads were preincubated in PBS at 4°C overnight, and then 293T cell lysis buffer was incubated in GST-binding buffer with streptavidin Sepharose beads at 4°C for 4

hours. The beads were collected and washed using washing buffer (50 mM Tris-HCl, pH 7.4, 150 mM NaCl, 0.5% NP-40) five times, and the immunoprecipitates were analyzed by western blotting using the indicated antibody.

Animal experiments

5×10^6 A375 tumor cells were subcutaneously injected into the left oxter of female BALB/c nude mice. Tumor growth was measured using a caliper every three or four days, and the tumor volume was calculated using the formula: tumor volume = length × width^2/2. Quantitative data were presented as means ± SEM $p < 0.05$ was considered statistically significant.

Microscale thermophoresis (MST) assay

MST assay was performed as described previously with slight modifications (Xie et al., 2018). Briefly, HeLa cells expressing GFP-tagged MRE11, ΔGAR or R572Q/R576Q were lysed into RIPA buffer (Solarbio). Cell extracts containing MRE11 or its mutants at a constant concentration were mixed with two-fold serial dilutions of purified GST-C1QBP (74-282 aa) in optimized MST buffer (50 mM Tris-HCl, pH 7.4, 150 mM NaCl, 10 mM $MgCl_2$, 0.05% Tween-20). After 15 minutes incubation at room temperature, reaction mixtures were enclosed in premium-coated glass capillaries and loaded into the instrument (Monolith NT.115, NanoTemper, Germany). The following measurement procedures and Kd value analysis were performed as detailed before (Xie et al., 2018).

Immunohistochemistry (IHC)

IHC was performed as described previously (Song et al., 2018), except that the following antibodies were used. The anti-C1QBP mouse monoclonal antibody was purchased from Abcam and the anti-MRE11 rabbit antibody was from Novus. After incubation with primary antibodies, the HRP-conjugated anti-mouse or rabbit secondary antibody (ZSGB-Bio) was applied and IHC slides were observed with Olympus BX51 microscope and Olympus DP73 CCD photographic system.

QUANTIFICATION AND STATISTICAL ANALYSIS

Each experiment was repeated three times or more. For Figures 5K and 5L, n represents the number of cells. All statistical calculations were performed using GraphPad Prism v.7.0 or Excel, and all statistics were evaluated by unpaired Student's t test. Quantitative data were presented as means ± SD or means ± SEM $p < 0.05$ was considered statistically significant. Statistical details can be found in the figure legends.

DATA AND CODE AVAILABILITY

The raw data have been deposited to Mendeley and are available at https://doi.org/10.17632/495fbz3p92.1.